Proximity effects and characteristic lengths in ferromagnet-superconductor structures

Klaus Halterman[1,2,*] and Oriol T. Valls[1,†]
[1]*School of Physics and Astronomy and Minnesota Supercomputer Institute, University of Minnesota, Minneapolis, Minnesota 55455-0149*
[2]*Sensor and Signal Sciences Division, Naval Air Warfare Center, China Lake, California 93555*
(Received 17 May 2002; revised manuscript received 3 September 2002; published 31 December 2002)

We present an extensive theoretical investigation of the proximity effects that occur in clean ferromagnet/superconductor (F/S) systems. We use a numerical method to solve self-consistently the Bogoliubov–de Gennes equations in the continuum. We obtain the pair amplitude and the local density of states, and use these results to extract the relevant lengths characterizing the leakage of superconductivity into the magnet and to study spin splitting into the superconductor. These phenomena are investigated as a function of parameters such as temperature, magnet polarization, interfacial scattering, sample size, and Fermi wave vector mismatch, all of which turn out to have important influence on the results. These results should help characterize and analyze future data and are shown to be in agreement with existing experiments.

DOI: 10.1103/PhysRevB.66.224516 PACS number(s): 74.50.+r, 74.25.Fy, 74.80.Fp

I. INTRODUCTION

The importance of understanding the characteristic length scales and geometrical effects inherent to heterostructures consisting of ferromagnets in electrical contact with superconductors has received a considerable reinforcement from the ever-increasing advances in nanofabrication technology. These advances have made it possible (see, e.g., Refs. 1–3) to fabricate high-quality nanostructures involving ferromagnets, as well as normal metals, and superconductors. In parallel, there has been significant progress in the development and refinement of tunneling spectroscopy techniques. Scanning tunneling microscopy (STM) allows one to locally probe the electronic density of states (DOS) of hybrid systems over atomic length scales with sub-meV sensitivity.

When a normal metal is in good contact with a superconductor, superconductivity is weakened in the superconductor and induced in the normal metal. When the normal metal is not magnetic, this phenomenon is the traditional[4] proximity effect which is described quantitatively via the pair amplitude $F(\mathbf{r})$, which encompasses the spatial dependence of pair correlations in the both the superconductor and normal metal. If the nonsuperconductor is a ferromagnet, the superconducting proximity effect is drastically modified by the finite exchange field. Furthermore, the magnetic material can induce spin polarization in the superconductor, resulting in a magnetic proximity effect. The study of the spatial variation of both the pair amplitude and the local DOS is fundamental to the understanding of these nanostructures.

When considering such inhomogeneous systems, there are multiple length scales involved that must be elucidated. At $T=0$ the phase coherence in a clean normal metal in contact with a superconductor decays inversely with distance from the interface, with a characteristic length $\xi_N(0)$, which is essentially infinite.[5] At finite temperatures, the phase coherence decays exponentially over a much-reduced distance $\xi_N(T)$.[4] Conversely, at low T, the pair correlations in the superconductor become depleted near the interface over a length scale given by the zero-temperature superconducting coherence length ξ_0, while for T close to T_c, Ginzburg-Landau theory[6] predicts that the depletion is governed by a length scale $\xi_S(T)$ that diverges at T_c. Although the essentials of the standard proximity effect have been well understood for a long time,[4] the length scales in the intermediate-temperature regimes have not been systematically or consistently studied for a normal-metal–superconductor bilayer system, although self-consistent microscopic calculations exist for layered structures,[7] and results within the quasiclassical[8] description have been obtained. Other predictions are limited by being based on phenomenological or non-self-consistent[25] approaches.

If the nonmagnetic normal metal is replaced with a ferromagnet (F/S junctions and structures), the relevant length scales in the problem are altered significantly. Naively, one would expect that all phase coherence would be lost in the magnet, since the superconductor and ferromagnet have opposite types of long-range ordering: a ferromagnet favors parallel spin alignment and acts as an effective pair breaker, while a superconductor is comprised of Cooper pairs with (in the ordinary s-wave pairing considered here) antiparallel spin alignment. However, a stable superconducting state can arise in the ferromagnet in which the Cooper pairs have a net center-of-mass momentum.[9] The spin splitting in the ferromagnet introduces a new length scale ξ_2 set by the difference in the spin-up and spin-down Fermi wave vectors $\xi_2 \propto (k_{F\uparrow} - k_{F\downarrow})^{-1}$, typically much smaller than ξ_0.

An interesting manifestation of this effect is the π phase junction comprised of a ferromagnetic material sandwiched between superconductors.[10–12] This particular interplay of ferromagnetism and superconductivity has been studied for some time.[13–15] The peculiar oscillatory state (originally introduced in the context of a new superconducting state that arises in when magnetic impurities are present[16,17]) leads, in the sandwich geometry, to a nonmonotonic dependence of the critical temperature on the ferromagnet layer thickness.[18–21] Other works[22] have focused on the variation of the Josephson current with temperature. For certain values of the exchange field, spontaneous currents[23] may arise in F/S heterostructures.

For heterostructure configurations in which any of the ma-

terial thicknesses are of order of or smaller than the largest of the relevant intrinsic lengths, size effects will play a role, and the finite thicknesses of the layers become important geometric lengths in the proximity effects. It is then clearly preferable to tackle the problem using a theory which does not involve coarse graining over atomic length scales. It has been shown that in thin superconductor–normal-metal bilayers, interlayer resistance plays a key part.[24] Variations in the local DOS were calculated as a function of ferromagnet thickness.[25,26] These calculations were all based on the quasiclassical Usadel[27] or Eilenberger[28] equations. The use of quasiclassical techniques may not be appropriate when the thickness of the materials is only of a few atomic layers. Also, the Usadel equations are restricted to the limit when the mean free path is much smaller than any other relevant length scale in the problem, and therefore their use in these situations is questionable. It is therefore desirable to study finite-sized systems using a microscopic, self-consistent theory that can accurately account for these geometrical effects.

We are aware of no work that addresses the influence on the proximity effect of the mismatch between the three Fermi energies (or Fermi wave vectors) present in F/S junctions (corresponding to the superconductor, and to the up and down spin bands in the magnet). Previous work[29] on this question was limited to the case of nonmagnetic metal, at temperatures near T_c. It was found that when the Fermi wave vector in the normal side is smaller than that in the superconductor, a strong suppression of the pair amplitude in the normal metal ensues. Also for nonmagnetic materials, the DOS was studied[7] using a microscopic formalism that allowed for different Fermi wave vectors, in the context of layered short-coherence-length superconducting structures, but there was no systematic study. Therefore this influence is still an open question in the full parameter range. For F/S junctions, the influence of Fermi wave vector mismatches on the proximity effect is virtually uncharted territory. Spectroscopy studies[30] revealed a nontrivial dependence of the conductance spectrum on Fermi wave vector mismatch; however, the proximity effect was ignored there and the calculation was not self-consistent.

Another relevant quantity that has a strong influence on the proximity effects and which has been insufficiently studied is the interfacial scattering strength. The variation of T_c with interface scattering strength was calculated,[31] and the influence of interface scattering was investigated experimentally[32,33] for $S/F/S$ structures. High-sensitivity transport measurements[32] revealed that interface barrier strength was an important parameter. Since appreciable scattering at the interface should lead to a reduction in $F(\mathbf{r})$ near the interface, this is another example where a systematic, self-consistent solution to this problem is needed.

The main aim of this paper is therefore to present the main results of a comprehensive theoretical investigation of the influence of these many relevant parameters on the F/S proximity effects. We will use for these purposes a very recently developed numerical method that allows for an exact *self-consistent* solution of the relevant microscopic equations in the ballistic limit. The approach is based on numerically solving the continuum Bogoliubov–de Gennes (BdG) equations[6] for the quasiparticle amplitudes and energies. The method of numerical self-consistent solution has been described in Ref. 34 where results for particular limits (zero temperature, no barrier or mismatch, and semi-infinite geometry) were given. Finding the dependence of the F/S proximity effects on temperature and other parameters will thus be a part of our task here. These numerical procedures allow for the study of coherence lengths much longer than those one can consider in lattice real-space models.[35,36] It was shown[34] that for F/S junctions there is, besides the usual characteristic spatial period ξ_2, another length scale $\xi_1 \approx \xi_2$ which describes the fast decay of $F(\mathbf{r})$ very near the interface.

Our objective is to investigate the length scales characterizing the F/S proximity effects in both bulk and finite-sized junctions consisting of a ferromagnet of varying polarization, in contact with a superconductor. As alluded to above, the often extreme differences in length scales in the problem require a self-consistent microscopic theory that can deal with them simultaneously without the approximations inherent to quasiclassical and dirty-limit equations. We shall consider here several areas in parameter space highlighting the effects of temperature, Fermi energy mismatch, interfacial scattering, and finite sample size. Results will be given for the pair amplitude and for the local DOS for both bulk and finite heterostructures, and thus we will analyze the various length scales involved.

Although the objective of our study is to stimulate new experiments and to help analyze and characterize the resulting data, we particularly aim also here to make contact with existing experimental work. Recent STM measurements[37] indicate a clear modification to the normal metal density of states for a Nb-Au junction, as a function of superconductor width. We compare our results with these data using a bilayer model in which both the normal metal and superconductor have widths of order ξ_0. We also compare our theoretical results with tunneling data[3] from a F/S (Ni-Al) junction in which local DOS measurements were taken in the superconductor. The relatively large exchange energy of Ni makes it an ideal candidate for investigating the effect of magnetism on the pairing correlations in the superconductor. In both cases, we find, using relevant values of the parameters describing the materials used and the geometry of the experimental setup, very good agreement between theory and experiment.

The rest of this paper is organized as follows. In Sec. II, we outline the method of self-consistent solution to the problem. In Sec. III, we present our results for the numerous parameters discussed above for different geometries and compare our results with recent tunnel spectroscopy data. Finally in Sec. IV we summarize our conclusions.

II. METHOD

In this section we briefly review the spin-dependent microscopic BdG equations in our geometry and then outline the numerical method used for solving them. We also explain the procedure for calculating physical quantities paramount

in the study of proximity effects: namely, the pair amplitude and the local DOS. Most of the techniques used here follow those of Ref. 34. We will omit most of the details given there and focus our attention on those points where the methods employed depart from those developed in that work, such as the inclusion of an insulating barrier and of finite temperatures.

The BdG equations[6] are a conceptually simple and convenient set of microscopic equations used for studying inhomogeneous superconducting systems, in our case structures involving, in addition to the superconductor, a ferromagnet. We consider a particular slablike geometry where the materials are assumed to extend to infinity in the x-y plane and have a total arbitrary thickness d along the z direction, where the only geometrical variation occurs. We denote the thicknesses of the ferromagnetic and superconducting layers by d' and $d-d'$, respectively. These materials are in general separated by a thin insulating barrier at $z=d'$. Since in this geometry the system is translationally invariant in the x-y plane, some aspects of the problem are effectively one dimensional. For this configuration, we then have two sets of coupled equations, one for the spin-up and spin-down quasiparticle and quasihole wave functions $(u_n^{\uparrow},v_n^{\downarrow})$, and another for $(u_n^{\downarrow},v_n^{\uparrow})$. The first takes the form[6,34] ($\hbar=k_B=1$)

$$\left[-\frac{1}{2m}\frac{\partial^2}{\partial z^2}+\varepsilon_{\perp}+U(z)-E_F(z)-h_0(z)\right]u_n^{\uparrow}(z)+\Delta(z)v_n^{\downarrow}(z)=\epsilon_n u_n^{\uparrow}(z), \tag{1a}$$

$$-\left[-\frac{1}{2m}\frac{\partial^2}{\partial z^2}+\varepsilon_{\perp}+U(z)-E_F(z)+h_0(z)\right]v_n^{\downarrow}(z)+\Delta(z)u_n^{\uparrow}(z)=\epsilon_n v_n^{\downarrow}(z), \tag{1b}$$

where $\varepsilon_{\perp}$ is the transverse kinetic energy, ϵ_n are the quasiparticle energy eigenvalues (the index n labels the relevant quantum numbers), and $h_0(z)=h_0\Theta(z-d')$ is the magnetic exchange energy. Scattering at the interface (assumed to be spin independent) is accounted for by the potential $U(z)=H\delta(z-d')$, where H is the barrier strength parameter. The pair potential $\Delta(z)$ satisfies a self-consistency condition as discussed below, and since we will assume that there is no current flowing in the system, we can take it to be real. In general, we must allow for the possibility of having up to three different Fermi wave vectors or bandwidths[30] in the problem. The quantity $E_F(z)$ equals E_{FM} in the magnetic side, $0<z<d'$, so that $E_{F\uparrow}=E_{FM}+h_0$ and $E_{F\downarrow}=E_{FM}-h_0$, while in the superconducting side, $d'<z<d$, $E_F(z)=E_{FS}$. We will be assuming parabolic bands so that $\varepsilon_{\perp}=1/2m(k_x^2+k_y^2)$ and there are three Fermi wave vectors, corresponding to $E_{F\uparrow}$, $E_{F\downarrow}$, and E_{FS}. The solutions for the other set of wave functions $(u_n^{\downarrow},v_n^{\uparrow})$ are easily obtained from those of Eqs. (1) by allowing for both positive and negative energies, and then using the transformation $u_n^{\uparrow}\rightarrow v_n^{\uparrow}, v_n^{\downarrow}\rightarrow -u_n^{\downarrow}, \epsilon_n\rightarrow-\epsilon_n$.

Equations (1) must be solved in conjunction with the self-consistency condition for the pair potential,

$$\Delta(z)=\frac{g(z)}{2}{\sum_n}'\,[u_n^{\uparrow}(z)v_n^{\downarrow}(z)+u_n^{\downarrow}(z)v_n^{\uparrow}(z)]\tanh(\epsilon_n/2T), \tag{2}$$

where T is the temperature and $g(z)$ is the effective BCS coupling constant, which will be taken to be zero outside the superconductor and a constant within it. The prime on the sum in Eq. (2) indicates that the sum is restricted to eigenstates with $|\epsilon_n|\leqslant\omega_D$, where ω_D is the Debye energy.

We now solve Eqs. (1) by expanding the quasiparticle amplitudes in terms of a complete set of functions $\phi_q(z)$,

$$u_n^{\uparrow}(z)=\sum_q^N u_{nq}^{\uparrow}\phi_q(z),\quad v_n^{\downarrow}(z)=\sum_q^N v_{nq}^{\downarrow}\phi_q(z). \tag{3}$$

We will use the normalized particle in a box wave functions $\phi_q(z)=\sqrt{2/d}\sin(k_q z)$ as our choice for the complete set. Here $k_q=q/\pi d$ and q is a positive integer. The finite range of the pairing interaction ω_D permits the sums in Eqs. (3) to be cut off at an integer N as discussed in Ref. 34, in a way that depends on the maximum wave vector present. Upon inserting the expansions (3) into Eqs. (1) and making use of the orthogonality of the $\phi_q(z)$, we arrive at the following $2N\times 2N$ matrix eigensystem:

$$\begin{bmatrix} H^{+} & D \\ D & H^{-}\end{bmatrix}\Psi_n=\epsilon_n\Psi_n, \tag{4}$$

where Ψ_n is the column vector corresponding to $\Psi_n^T=(u_{n1}^{\uparrow},\ldots,u_{nN}^{\uparrow},v_{n1}^{\downarrow},\ldots,v_{nN}^{\downarrow})$. The matrix elements are given by

$$H_{qq'}^{+}=\left[\frac{k_q^2}{2m}+\varepsilon_{\perp}\right]\delta_{qq'}+\int_0^d dz\,\phi_q(z)U(z)\phi_{q'}(z)-E_{F\uparrow}\int_0^{d'}dz\,\phi_q(z)\phi_{q'}(z)-E_{FS}\int_{d'}^{d}dz\,\phi_q(z)\phi_{q'}(z), \tag{5a}$$

$$H_{qq'}^{-}=-\left[\frac{k_q^2}{2m}+\varepsilon_{\perp}\right]\delta_{qq'}-\int_0^d dz\,\phi_q(z)U(z)\phi_{q'}(z)+E_{F\downarrow}\int_0^{d'}dz\,\phi_q(z)\phi_{q'}(z)+E_{FS}\int_{d'}^{d}dz\,\phi_q(z)\phi_{q'}(z), \tag{5b}$$

$$D_{qq'}=\int_{d'}^{d}dz\,\phi_q(z)\Delta(z)\phi_{q'}(z). \tag{5c}$$

The self-consistency condition is now transformed into

$$\Delta(z)=\frac{g(z)}{2}\sum_{p,p'}{\sum_n}'\,[u_{np}^{\uparrow}v_{np'}^{\downarrow},\phi_p(z)\phi_{p'}(z)+u_{np}^{\downarrow}v_{np'}^{\uparrow},\phi_p(z)\phi_{p'}(z)]\tanh(\epsilon_n/2T), \tag{6}$$

where the sum over the quantum numbers n encompasses a sum over the continuous transverse energy $\varepsilon_{\perp}$ and a quantized longitudinal momentum index q,

$$\sum_n{}' \rightarrow \sum_{\varepsilon_\perp}{}' \sum_q{}' . \tag{7}$$

The matrix eigensystem Eq. (4) and the self-consistency condition (6) constitute the primary equations drawn upon in this paper. They are solved numerically, using the algorithm developed and described in previous work.[34] The iterative computational process is completed when the maximum relative error in $\Delta(z)$ between successive iterations is less than a prescribed value as explained below.

Once we have the self-consistently calculated eigenvalues and eigenvectors, we can then construct all relevant physical quantities. For example, the usual penetration depths are conveniently obtained from the pair amplitude $F(z)$,

$$F(z)=\Delta(z)/g(z). \tag{8}$$

The pair amplitude, unlike $\Delta(z)$, is therefore not restricted by the coupling constant to vanish in the nonsuperconductor. $F(z)$ gives a quantitative measure of the superconducting correlations in both the superconductor and nonsuperconductor where there may exist phase coherence between particle and hole wave functions. The value of $F(z)$ in the nonsuperconducting region, however, does not affect the quasiparticle dynamics since it is only $\Delta(z)$ that enters into the BdG equations.

We can also use our numerical results for the excitation spectra to calculate the experimentally accessible local single-particle properties via the thermally broadened DOS

$$N(z,\varepsilon)=N_\uparrow(z,\varepsilon)+N_\downarrow(z,\varepsilon), \tag{9}$$

where the local DOS for each spin state is given by[38]

$$N_\uparrow(z,\epsilon)=-\sum_{p,p'}\sum_n{}' [u^\uparrow_{np}u^\uparrow_{np'}\phi_p(z)\phi_{p'}(z)f'(\epsilon-\epsilon_n) + v^\uparrow_{np}v^\uparrow_{np'}\phi_p(z)\phi_{p'}(z)f'(\epsilon+\epsilon_n)], \tag{10a}$$

$$N_\downarrow(z,\epsilon)=-\sum_{p,p'}\sum_n{}' [u^\downarrow_{np}u^\downarrow_{np'}\phi_p(z)\phi_{p'}(z)f'(\epsilon-\epsilon_n) + v^\downarrow_{np}v^\downarrow_{np'}\phi_p(z)\phi_{p'}(z)f'(\epsilon+\epsilon_n)]. \tag{10b}$$

Here $f'(\epsilon)=\partial f/\partial\epsilon$ is the derivative of the Fermi function. We will also be interested in the quantity

$$\delta N(z,\varepsilon)=N_\uparrow(z,\varepsilon)-N_\downarrow(z,\varepsilon), \tag{11}$$

which will be used to characterize the effective leakage of magnetism into the superconductor.

III. RESULTS

In this section, we present numerical results for the pair amplitude and local DOS, and discuss other physically meaningful quantities arising from the self-consistent excitation spectra. We will analyze the various length scales characterizing the influence of the superconductor on the ferromagnet and vice versa. We divide this section into four different subsections dealing with the following topics: (1) systematics of the temperature, exchange field, Fermi wave vector mismatch, and barrier height for bulk F/S systems; (2) dependence of the results on the finite thickness of either the F or the S layer; and finally (3) a comparison with experimental results. Most of the results are conveniently expressed in terms of the dimensionless quantities compactly defined and listed in Table I. Unless otherwise indicated, we use $\omega=0.1$ for the Debye cutoff in units of E_{FS} and $\Xi_0 \equiv k_{FS}\xi_0=50$ in this work. All lengths z are measured in units of the inverse of k_{FS}. For example, the widths of the ferromagnet or superconductor layers are represented as $D_F=k_{FS}d'$ and $D_S=k_{FS}(d-d')$. The bulk case is studied by choosing values of D_S and D_F sufficiently large so that the results become independent of these quantities.

TABLE I. Dimensionless variables.

Physical quantity	Dimensionless form
Exchange energy	$I\equiv h_0/E_{FM}$
Fermi wave vector mismatch	$\Lambda\equiv(k_{FM}/k_{FS})^2$
Temperature	$t\equiv T/T_c$
Coherence length	$\Xi_0\equiv k_{FS}\xi_0$
Debye energy	$\omega\equiv\omega_D/E_{FS}$
Barrier strength	$H_B\equiv mH/k_{FM}$
Distance relative to interface	$Z\equiv k_{FS}(z-d')$

As mentioned above, we employ a numerical algorithm as in Ref. 34 to solve the self-consistent eigenvalue problem, Eqs. (4) and (6). The procedure involves making a reasonable initial guess for $\Delta(z)$, where the coordinate z is of course discretized for numerical purposes. The initial guess may be taken to be a previously obtained converged result corresponding to a slightly different set of parameter values or, in the absence of any such suitable previous result, a step function, e.g., $\Delta(Z)=\Delta_0\Theta(Z)$, where Z is the dimensionless distance from the interface (see Table I) and Δ_0 the bulk value of the gap at $T=0$. We then diagonalize the $2N\times 2N$ matrix described by Eq. (4) for each value of $\varepsilon_\perp$. The cutoff number N, as explained in Ref. 34, depends chiefly on $D\equiv k_{FX}d$, where k_{FX} is the largest Fermi wave vector in the problem and d the total thickness, which is up to $1200k_{FS}^{-1}$ in our calculations. We use 5000 different values of $\varepsilon_\perp$ consistent with the energy cutoff. The value 5000 is 5–10 times larger than that used in previous work, which makes for better convergence and smoother results. Self-consistency is achieved[34] via an iteration process. The process terminates when the relative error between successive $\Delta(z)$ is less than a suitable number, chosen here to be 10^{-4} (one-tenth of the criterion in previous work). The pair potential settles down, after starting with a step function initial guess, to its self-consistent form within about 25 iterations. This value is typical for most parameter values and system sizes used in this paper. The only exceptions are when the temperature approaches T_c (the bulk transition temperature of the superconductor) or when the superconductor width is of order of ξ_0. Then the number of iterations needed for self-consistency is much larger (up to several hundred) if one starts with a step function guess for $\Delta(Z)$. This problem can be alleviated by

calculating $\Delta(z)$ self-consistently for a given temperature and then use this as input for a nearby temperature as described above.

A. Parameter dependence

We consider in this subsection the main highlights of the dependence of our results on temperature and on material parameters (exchange field, wave vector mismatch, and barrier height), in the limit where both ferromagnet and superconductor are very thick (''bulk'' limit). By this we mean that both D_F and D_S are taken to exceed the temperature-dependent coherence length. In this subsection we have taken $D_F = D_S = 12\Xi_0$ (recall $\Xi_0 = 50$), so that $D_F, D_S \gg \Xi_0$, and we are in the bulk limit except extremely close to T_c, $t \lesssim 0.99$. We subdivide the analysis into three categories that address, respectively, temperature and exchange effects, Fermi energy mismatch, and interfacial scattering effects.

We will focus here on the results for $I \neq 0$. We have, however, extensively studied[39] the limit ($I=0$) where the nonsuperconducting material is nonmagnetic and verified that previously known results for this well-studied case are reproduced.

1. Temperature and exchange energy dependence

We now study how variation of the temperature affects the pair amplitude and local DOS at finite values of the dimensionless exchange energy I. To isolate these effects, we assume that there is no interface barrier and no Fermi energy mismatch ($\Lambda = 1$, $H_B = 0$; see Table I). We consider first the pair amplitude $F(Z)$. At $I=0$ this quantity has a very slow decay into the normal region and at $T=0$ is expected[5] to decay as the inverse of the distance from the interface,

$$F(Z) = \frac{c_1}{|Z| + c_2}, \tag{12}$$

where c_1 and c_2 are constants. We find[39] that the expression, Eq. (12), is valid, but only very close to the interface. Upon increasing T, the relevant length scale in the normal metal is set by[4] $\xi_N(T) = v_{FM}/2\pi T$, where $v_{FM} \equiv k_{FM}/m$. As T increases the length scale characterizing the decay of $F(Z)$ decreases, and that at a fixed, finite temperature it cannot be fit to a single exponential. For temperatures close to T_c, an approximate form for the pair amplitude has been given as[4]

$$F(Z) = \Phi(Z)\exp[-|Z|/\xi_N(T)], \tag{13}$$

where $\Phi(Z)$ is a slowly varying function. Our results[39] agree with Eq. (13) in the temperature regime near T_c ($t > 0.9$) and for sufficiently large $|Z|$ ($|Z| > \Xi_0$). On the superconductor side, as the temperature is increased, the depletion of superconducting correlations occurs over a length scale which increases with T. We denote this scale (in units of inverse k_{FS}) by $\xi_S(T)$. Close to T_c the profile for the pair amplitude is well known from standard Ginzburg-Landau (GL) theory[6] to be given by a hyperbolic tangent form. Our results[39] fit the GL expression adequately for temperatures $T \lesssim T_c$. As the temperature is decreased, the GL expression remains an adequate fit within a region of at least one coherence length from the interface. For most of the temperature range, the characteristic length ξ_S fits well to the GL expression $\xi_S(T) = 0.74\Xi_0(1-t)^{-1/2}$. Thus, our limiting results are in agreement with previous theory and expectations for the standard (nonmagnetic) proximity effect and we can proceed with confidence to the more interesting case where the exchange energy parameter I is finite.

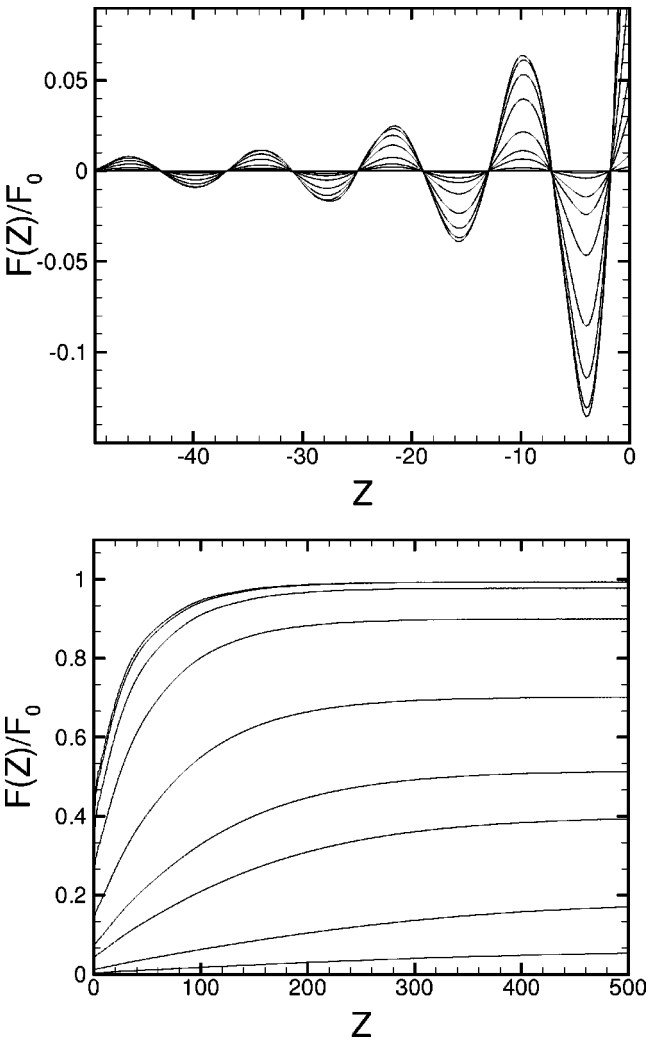

FIG. 1. The pair amplitude $F(z)$, normalized to the zero-T bulk value $F_0 = \Delta_0/g$ in the superconductor, plotted as a function of dimensionless distance $Z = k_{FS}z$ from the interface. Results are for $I = 1/2$. The top panel depicts the magnetic region, while the bottom panel shows the superconducting region. The curves correspond, from top to bottom on the superconducting side or in order of decreasing amplitude in the magnetic side, to temperatures $t \equiv T/T_c = 0, 0.2, 0.4, 0.6, 0.8, 0.9, 0.94, 0.98, 0.99$. Note the different vertical and horizontal scales used in both panels.

In Fig. 1, the pair amplitude $F(Z)$ is shown in the magnetic and superconductor sides (top and bottom panels, respectively) for a wide range of temperatures, at the intermediate value $I = 1/2$. In all plots for this quantity, we normalize $F(Z)$ to the zero T bulk value $F_0 = \Delta_0/g$. The two regions $Z > 0$ (superconductor) and $Z < 0$ (normal) are plotted in separate panels because their significant features occur over different length and vertical scales. The pair amplitude, how-

ever, is always continuous across the interface. We see that on the magnetic side (upper panel), $F(Z)$ has an oscillatory behavior, very different from the monotonic behavior at $I=0$. This is because when an exchange field is present the spin degeneracy that existed for $I=0$ is removed. The result is that the Fermi wave vectors of the spin-up and spin-down electrons, $k_{F\uparrow}, k_{F\downarrow}$, are different, and consequently a Cooper pair entering the ferromagnet acquires a net center-of-mass momentum. The superconducting order induced in the ferromagnet arises from the product of particle and hole wave functions [e.g., $u_n^{\uparrow}(z)v_n^{\downarrow}(z)$] summed over all quantum numbers n. It is the superposition of these wave functions that causes the superconducting wave function to oscillate[9] on a length scale set by the difference in the spin-up and spin-down wave vectors, $\xi_2 \approx (k_{F\uparrow}-k_{F\downarrow})^{-1}$. We have

$$k_{FS}\xi_2 = \frac{1}{[\Lambda(1+I)]^{1/2}} k_{F\uparrow}\xi_2, \tag{14}$$

where Λ is the wave vector mismatch parameter of Table I. Since[34] $k_{F\uparrow}\xi_2 \approx 1/I$, we see from this figure and similar results for other values of I that the characteristic length of oscillations scales as $1/I$, and therefore, except at extremely small I, it is much smaller than length scale set in the normal metal case above.

We have previously studied[34] the explicit form for the pair amplitude in the ferromagnet at zero temperature. We found that for most exchange fields and except extremely near the interface, the pair amplitude is given by

$$F(Z) = \alpha \frac{\sin[Z/(k_{FS}\xi_2)]}{Z/(k_{FS}\xi_2)}, \quad T=0, \tag{15}$$

where α is a constant. Very close to the interface, the pair amplitude monotonically decays over a characteristic length ξ_1 which is defined as the first point inside the ferromagnet at which $F(Z)$ is zero. The length scale ξ_1 goes also as $k_{FS}\xi_1 \approx 1/I$.

We are interested in how the pair amplitude and various characteristic lengths associated with it are modified as T increases, at finite I. Starting with the largest amplitude curve in the upper panel of Fig. 1 ($T=0$), we see that, beyond a small region of fast decay at the interface, the pair amplitude exhibits damped oscillations, with a temperature independent period that coincides with the expected value $k_{FS}\xi_2 \approx 1/I = 2$, independent of T. The envelope decay of the oscillations varies inversely with distance as given in Eq. (15). The quantity ξ_1 is also independent of temperature, since as can be seen in the figure the location of the first node of $F(Z)$ as it monotonically goes to zero near the interface is the same for all temperatures. As T increases, however, the amplitude of the oscillations in $F(Z)$ markedly decreases. This decrease, as we shall see below, is not merely a reflection of the smaller value of $\Delta(T)$ in the bulk superconductor. Because of this competition between thermal and exchange energies, the pair amplitude now has a slightly more complicated functional form than that given by Eq. (15). We find that in order to fit our numerical results, Eq. (15) must be modified by incorporating additional spatial- and temperature-dependent factors. The amplitude of the oscillatory decay of $F(Z)$ no longer decays as the inverse distance from the interface, but now has an additional slowly varying exponential term $\Phi'(Z)$ and a purely temperature-dependent amplitude $A(t)$,

$$F(Z) = A(t)\Phi'(Z)\frac{\sin[(Z+\theta)/k_{FS}\xi_2]}{(Z+\theta)/k_{FS}\xi_2}, \tag{16}$$

where θ is a small, weakly I-dependent shift that accounts for the sharp monotonic decay right at the interface into the ferromagnet. We find that Eq. (16) holds for nearly the entire range values of I $0 \leqslant I \leqslant 1$. Certain exceptions occur in the extreme cases of very small $I \simeq \Delta_0/E_{FM}$ or very large $I \simeq 1$ and will be addressed below. The form of $A(t)$ in Eq. (16), is fitted well by the form $A(t)=A(0)(1-t^2)$. Thus $A(t)$ decreases faster with temperature than the bulk $\Delta(T)$, which shows that the decrease of the amplitude with temperature is not merely a normalization effect but involves an intrinsic decrease of the pairing at the interface. Temperature has a marked effect on the amplitude, but it does *not* wash out the oscillations themselves, which remain quite well defined even at temperatures quite close to T_c.

The superconductor side (bottom panel of Fig. 1) shows a behavior of $F(Z)$ very similar to that in the $I=0$ case, with the variation of $F(Z)$ again occurring over the length scale $\xi_S(T)$. The very slight wiggles in $F(Z)$ which may be observed near the interface are due to the increased mismatch of the two Fermi energy levels in the ferromagnet with E_{FS}. The effect of the exchange field on $F(Z)$ in the superconductor region therefore seems to be minimal at all temperatures. We will see, however, that the pair amplitude is only partially useful in conveying the total effect of magnetism leakage into the superconductor. The quantity $\delta N(z)$ from Eq. (11) will be used below for extracting additional useful information on this question.

In the extreme (half metallic) case of $I=1$, where only one spin band is present in the ferromagnet at the Fermi level, the characteristic length scale that describes the main oscillatory behavior is still given from Eq. (14) as $k_{FS}\xi_2 = 1/\sqrt{2}$ (recall that we are using $\Lambda=1$ in this subsection). The relevant spatial variations occur now only on an atomic scale. This reflects that Andreev processes are inhibited by the absence of Fermi level down states deep within the magnet. One then finds[39] clear deviations from the pure damped sinusoidal behavior seen for smaller exchange field values. The superconducting region follows the same pattern as the other cases, but very near the interface there exist small oscillations of order of the Fermi wavelength. The oscillations were barely glimpsed at $I=1/2$ and disappear with decreasing I.

The pair amplitude at the interface at constant temperature decreases markedly with I, while at constant I it decreases with T. The minimum value Δ_{MIN} of the normalized $\Delta(Z)$ in the superconductor occurs right at the interface, and because of the relatively wide horizontal scale in the bottom panels of Fig. 1, it is not possible to read its value from that figure. The effect of the exchange field on Δ_{MIN} turns out to be quite pronounced, and as the temperature approaches T_c, Δ_{MIN} vs t curves tend to collapse into a nearly straight line, tending to

zero at $t=1$. The superconducting correlations at the interface are also obviously depleted as I increases.

It is now pertinent to examine the local density of states at various positions on both sides of the interface. The local DOS gives further direct insight into the proximity effect, and more important, it is an experimentally accessible quantity. Its calculation is achieved through Eq. (9) and the computed self-consistent spectra.

At $I=0$, our method reproduces, for the local DOS at low temperature within the normal metal region, the sawtoothlike pattern characteristic of the de Gennes–St. James states as predicted long ago.[40] The DOS is small but finite at the Fermi energy due to filling by thermally excited quasiparticles and then rises nearly linearly at small energies. The Andreev bound states result in peaks in the DOS. These are due to constructive interference of the electron and hole wave functions, as they undergo Andreev reflection at the F/S interface and normal reflection at the vacuum–normal-metal interface at the opposite end of the sample. The characteristic energy E_c of the peaks is determined by adding up the phases for a given trajectory.[41] In agreement with theoretical expectations, we find that the first peak occurs at an energy $E_c \approx \pi v_{FM}/4d' \approx 0.2\Delta_0$, while the other peaks occur approximately at multiples of $2E_c$. The energy scale E_c can be seen directly in the calculated self-consistent energy spectrum.[39] In the energy region below the gap ($\epsilon/\Delta_0<1$), it is found that for nearly longitudinal momenta ($\varepsilon_\perp \approx 0$), there exist roughly three excitation branches, at the same energies as the peaks seen in the local DOS. The width of the peaks is due to the numerous quasiparticle states with momenta nearly perpendicular to the interface. The bound states diminish as one moves further into the superconductor, and there are no longer any states at the Fermi energy. Increasing the temperature tends to smear the lower-T results.

The effect of I on the local DOS is very drastic, as seen in Fig. 2, which shows results for the local DOS (normalized, as will be our convention in this work, to its normal-state Fermi level value in the superconducting material) for $I=1/2$, at several positions. The above discussed bound-state phenomena, seen at $I=0$ in the normal side relatively far from the interface, are no longer observable at $I=1/2$ because the overall decay of superconducting correlations takes place over considerably smaller distances. On the other hand, this decay takes place now in a nonmonotonic matter, which gives rise to a new set of features in the ferromagnet, very near the interface: in the left column of Fig. 2 we show the local DOS at four positions at and very near the interface. The influence of the oscillatory pair amplitude (Fig. 1) becomes evident as we examine the four plots in this column. The subgap structure in the top curve ($Z=-3$) evolves so that maxima and minima become reversed at $Z=-1$, closer to the interface. The same occurs for $Z=-2$ and $Z=0$. Comparing with Fig. 1, we see that the oscillating superconducting order has in effect induced oscillations in the local DOS as a function of position within the ferromagnet and that the large exchange field induces noticeable particle-hole asymmetry. The length scale at which the DOS flips ($\Delta Z=2$) coincides with the characteristic distance $k_{FS}\xi_2$, given in Eq. (14). Although this figure depicts results obtained for

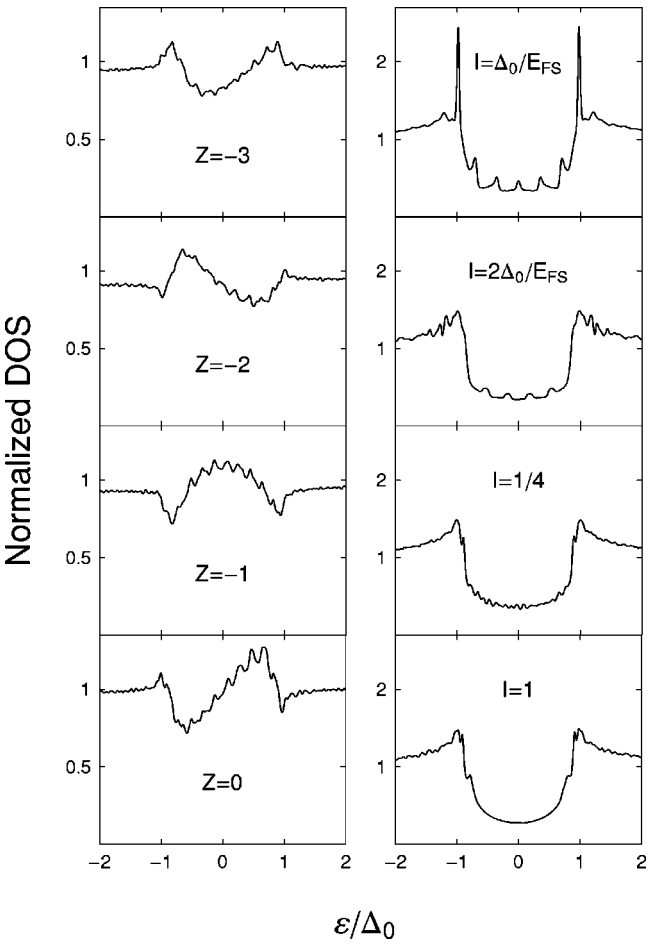

FIG. 2. Local DOS (normalized to its Fermi level value in the normal state of the superconductor), plotted vs dimensionless energy ϵ/Δ_0. The left column is for the case $I=1/2$ and $t=0.02$ at four positions near the interface. The right column corresponds to the various I values shown, at the fixed position $Z=50=\Xi_0$. The temperature is given by $t=0.02$.

a rather low temperature, the oscillatory behavior is never completely washed out by the temperature, as remarked above in conjunction with the discussion of $F(Z)$. The same behavior holds true *a fortiori* for the half metallic case $I=1$. One important difference between this and the intermediate I case is the spatial scale at which the DOS oscillations occur. Since $1/I=1$, the complete DOS inversion should occur at points separated by an interval δZ of order unity.

In the right column of Fig. 2 we consider the superconductor side of the junction: these panels display the local DOS one coherence length ξ_0 from the interface for four different exchange fields, at the temperature t=0.02. For the value of I in the top panel [$I=\Delta_0/E_{FS}$, which for the values of the parameters considered in this subsection, equals 0.0127, as can be seen from Table I and the BCS relation $k_F\xi_0=(2E_F)/(\pi\Delta_0)$], possible resonance effects have been predicted.[42] Focusing on energies $|\epsilon/\Delta_0|<1$, we see a dramatic jump in the DOS near the gap edge and five smaller peaks at lower energies. Upon doubling I, to $I=2\Delta_0/E_{FS}$, the sharp peak structure near $\epsilon/\Delta_0=1$ vanishes, and four smaller subgap peaks appear. Indeed, we have found that the

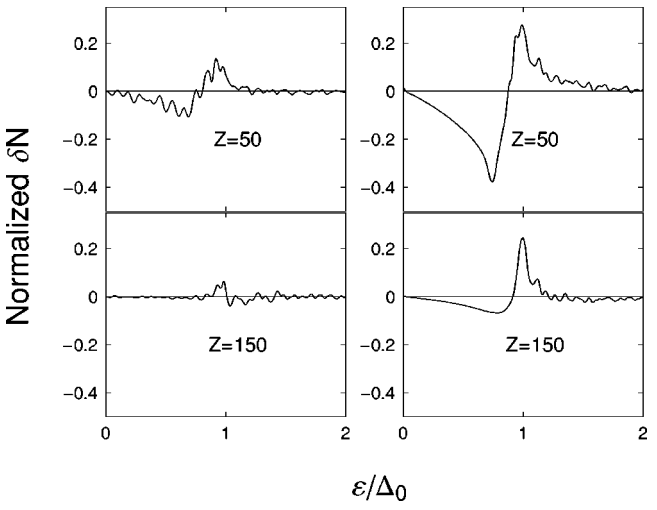

FIG. 3. The quantity δN [see Eq. (11)] normalized to the normal-state DOS summed over spins, plotted vs dimensionless energy at two indicated positions in the superconductor, for $I=0.25$ (left column) and $I=1$ (right column) at $t=0.02$.

sharp peak exists only at $I=\Delta_0/E_{FM}$. It would be of considerable interest to verify experimentally the appearance and disappearance of the very sharp peak at the gap edge for $I=\Delta_0/E_{FM}$. The third panel from the top ($I=1/4$) demonstrates a reduction in the interference patterns seen above. The smoothing effect of increased I is further exemplified below it for the half metallic case ($I=1$), where there is also a slight decrease in the number of states at the Fermi level ($\epsilon=0$). The four figures illustrate the near absence of DOS asymmetry in the superconductor.

Examination of results such as those displayed in the bottom (superconductor side) panels of Fig. 1 shows that the exchange field seems to affect the pair amplitude $F(Z)$ within the superconductor relatively little over any significant length scales. We want to study the possibility, however, that the differential local DOS $\delta N(\epsilon,z)$, defined in Eq. (11), may show, within the superconductor, magnetic penetration over distances much larger than that revealed by $\Delta(z)$. We have a hint that this might be the case: the results for $\Delta(z)$ in Ref. 34 exhibited no significant dependence on I, while $\delta N(\epsilon,z)$ was appreciably nonzero within a small region in the superconductor near the interface. These previous results were obtained for the special case where $k_{FS}=k_{F\uparrow}$, a condition which corresponds to an I-dependent mismatch parameter $\Lambda=1/(1+I)$, which may yield results different from the case $\Lambda=1$ considered here.

We examine spin polarization effects in the superconductor in Fig. 3, where we plot the normalized $\delta N(Z)$ [see Eq. (11)] for $I=1/4$ (left column) and $I=1$ (right column). We use $t=0.02$ and choose two locations in the superconductor, at $Z=\Xi_0$ and $Z=3\Xi_0$. At the position $Z=\Xi_0$ (top panels) there is a clear manifestation of the magnetic proximity effect through a nonzero value of δN near $\epsilon/\Delta_0=1$. The effect decreases as Z increases and, for $I=1/4$, it nearly dies out at $Z=3\,\Xi_0$. At $I=1$ (half metallic case) the effect is more prominent and extends over larger distances. However, the integral of δN over energies turns out to be always extremely small (as we shall see below) at these distances, at which only the self-consistent energy spectral distribution shows magnetic penetration spin-splitting effects. We see that δN vanishes at the Fermi level but the details of this fairly long-range redistribution of energy states are nontrivial and difficult to interpret. Nevertheless, that the effect is larger near the gap energy can be readily understood if one recalls that[43] the imaginary part of the wave vector of injected quasiparticles below the gap (in a non-self-consistent approach) vanishes as the gap edge is approached.

In previous work[34] it was found, as mentioned above, that for $I=1$ and no mismatch between the spin-up and superconductor band ($E_{F\uparrow}/E_{FS}=1$), the effect of the exchange field on the superconductor was small and $\delta N(Z)$ decayed away over a few atomic distances. However, the current condition $\Lambda=1$ implies, at $I=1/4$ and particularly at $I=1$, a considerable mismatch between k_{FS} and $k_{F\uparrow}$. We shall study this point in more detail below, in the context of our discussion of wave vector mismatch in general.

2. Fermi wave vector mismatch

In the last paragraph, we have seen that (as previously[30] seen in a different context) mismatch among the three Fermi wave vectors involved in the problem (or the three bandwidths) may have a considerable effect on the results. As such mismatch is experimentally unavoidable, we now proceed to investigate it in some detail. Thus, we will consider values of the mismatch parameter Λ (Table I) different from unity. We will still keep the interface barrier parameter at $H_B=0$. We focus on the situation where the bandwidth in the normal metal is smaller than that of the superconductor. This is the more common situation in F/S structures and, in any case, it turns out to lead to more prominent effects.

At $I=0$, the superconducting correlations decrease[39] as Λ decreases (that is, as the mismatch increases). At $\Lambda=0.1$ phase coherence is virtually destroyed at $Z=-200$ at low temperatures. Away from the interface, within the superconductor, the pair correlations still decay in accordance with Eq. (12), the only modification being that the amplitude factor $c_1(\Lambda)$ becomes mismatch dependent. Thus, a smaller bandwidth in the normal metal tends to restrict the influx of Cooper pairs. Physically, since the parallel momentum of a Cooper pair at interface is conserved, the longitudinal component is restricted by the smaller number of states accessible in the normal side.[29] This is consistent with the behavior of $F(Z)$ in the superconductor. The characteristic rise length in the superconductor now decreases with mismatch. However, $F(Z)$ remains continuous at the interface. The effects of values of Λ in the range $\Lambda>1$ are in the opposite direction, but always much less prominent. For this reason this range has been deemphasized.

The top panel of Fig. 4 displays the damped oscillations of $F(Z)$ in the magnet, at $I=1/2$. The period of the damped oscillations varies inversely with $\sqrt{\Lambda}$, in agreement with Eq. (14), but they nearly wash out when $\Lambda=0.1$. Also, the sharp monotonic decline very near the interface increases in slope with greater Λ, so that $F(Z)$ first reaches zero at a greater distance from $Z=0$, thus also increasing $k_{FS}\xi_1$ defined ear-

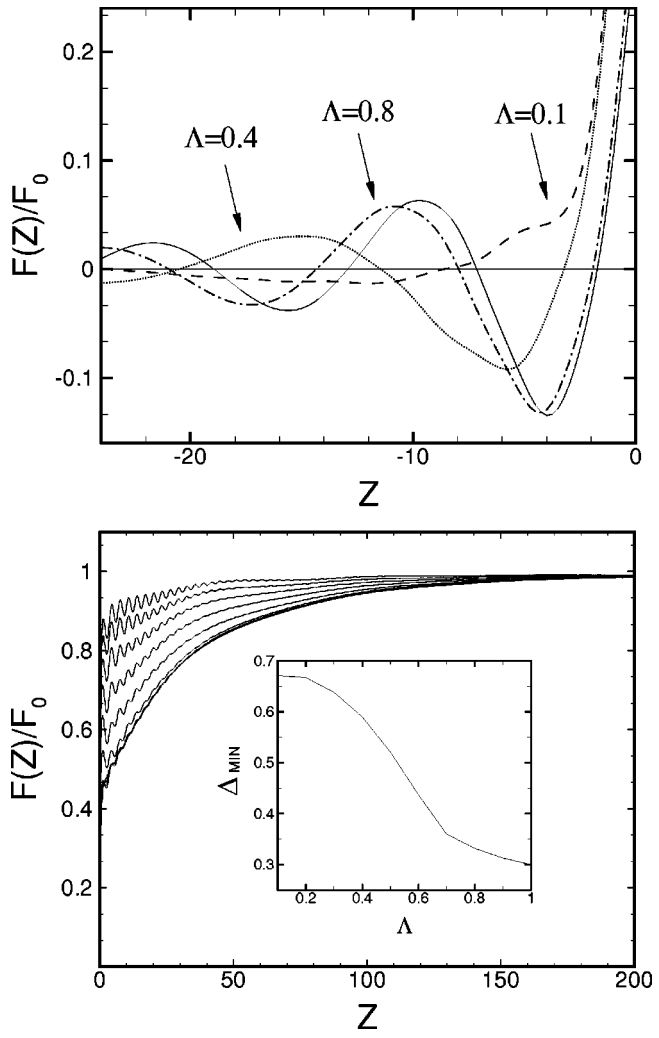

FIG. 4. Normalized pair amplitude for the case $I=1/2$ and $t=0.1$. The top panel illustrates the variation of $F(Z)$ for three different Λ (as indicated) in the ferromagnet, while in the superconductor side (bottom panel) results for values of the mismatch parameter Λ (see Table I) $\Lambda=0.1$–1, in increments of 1/10 (in order of decreasing Λ from top to bottom). The inset depicts the value of $\Delta(Z)$ at the interface, Δ_{MIN}, as a function of the parameter Λ.

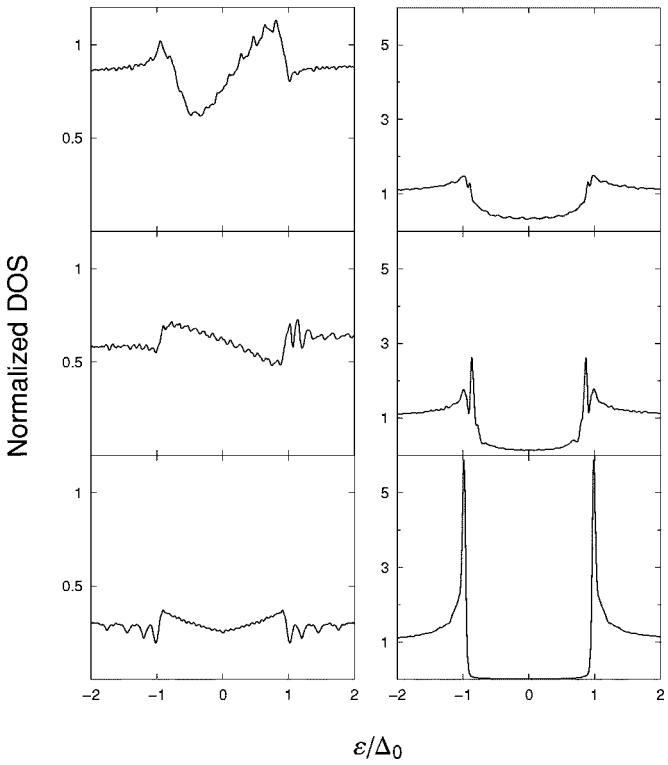

FIG. 5. Normalized local DOS plotted vs the dimensionless energy ϵ/Δ_0 at $I=1/2$ and $t=0.02$ for three values of the mismatch parameter $\Lambda=0.8,0.4,0.1$ (from top to bottom panels). The left column corresponds to the position $Z=-4$ in the ferromagnet, while the right column corresponds to $Z=\Xi_0$ in the superconductor.

lier. Quantitatively, one can obtain an excellent fit for the damped sinusoidal dependence of the pair amplitude by using Eq. (16) with $k_{FS}\xi_2$ as a fitting parameter. The results of doing this yield values in excellent agreement with Eq. (14).

In the bottom panel of Fig. 4, the top five curves show the drop in $F(Z)$ within the superconductor as the interface is approached. The main feature that stands out is that the results in the range $0.7<\Lambda<1$ are nearly independent of Λ, while those for $\Lambda<0.7$ exhibit a marked Λ dependence. This unexpected result arises as at $I=1/2$ and $\Lambda=2/3$ one reaches the special point where $E_{F\uparrow}=E_{FS}$. This property is further exemplified in the inset where we present Δ_{MIN} as a function of Λ. One can see a kink in the curve at about $\Lambda=2/3$.

The Fermi wave vector mismatch influences also the local DOS as we shall now show. At $I=0$, the main effect in the normal metal at low temperatures is that as Λ decreases (higher mismatch), the bound-state peaks decrease, until they disappear at $\Lambda=0.1$. The superconductor side shows an interesting trend. At a distance of order of one coherence length from the interface we find that, as one decreases Λ, the existing small but distinct peaks within the gap found at $\Lambda=1$ turn into small wiggles at $\Lambda=0.4$ and disappear altogether for $\Lambda=0.1$. The BCS peaks at the gap edge become much more pronounced, indicating a substantial reduction in Andreev reflection at the interface because of the increased mismatch in Fermi energies, which results in superconductivity being more ''confined'' to the superconductor.

We saw in the top panel Fig. 4 the effect of Λ on the damped oscillations of the pair amplitude. We investigate the corresponding effect on the DOS in the left column of Fig. 5 for the same values of I and Λ. There we depict the changes in the magnet side local DOS, with the coordinate fixed to $Z=-4$. As expected the DOS again experiences oscillations correlated with the characteristic length $k_{FS}\xi_2$, as a function of Λ. One can see an evident inversion between the $\Lambda=0.8$ and $\Lambda=0.4$ cases, whereby the positions of minima and maxima are interchanged. The superconductor side is examined in the right column, which shows the same Λ values as in the left set of panels, at a distance Z of one correlation length inside the material. The top panel exhibits behavior similar to that found for $\Lambda=1$: the density of states within the gap is appreciably nonvanishing, and the peaks at $\epsilon/\Delta_0=1$ are relatively low. The peaks near the gap edge for $\Lambda=0.4$ are more prominent and there is a concomitant decrease in subgap states. This is quantitatively different from

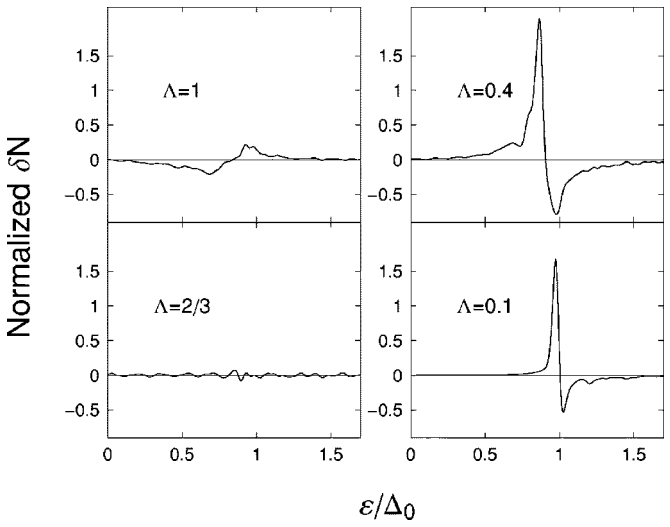

FIG. 6. Normalized δN at $Z=\Xi_0$ in the superconductor for different values of Λ, as labeled.

what we mentioned happens at $I=0$, where there are more subgap states and the BCS peaks are significantly sharper. Finally, the bottom panel reveals a near absence of states below the gap and the usual BCS-like peaks at $\epsilon/\Delta_0=1$.

It was also seen in Fig. 4 that $F(Z)$ in the superconductor decayed away from its bulk value near the interface in a strongly Λ-dependent manner. To address whether this parameter also affects the spin splitting in the superconductor, we now calculate $\delta N(z,\epsilon)$. Figure 6 shows δN (still at $t=0.02$ and normalized as previously) as a function of the dimensionless energy and at a distance of one ξ_0 from the interface, for several values of Λ, at $I=1/2$. Starting at $\Lambda=1$, we see an effect reminiscent of what was seen in Fig. 3: there is a net negative spin population for $\epsilon/\Delta_0 \lesssim 0.85$, then for larger energies, a greater number of up spin states, which decays quickly so that the two spin states equalize for $\epsilon/\Delta_0 > 1.5$. Next, consider the case where $\Lambda=2/3$ (when $k_{F\uparrow}=k_{FS}$). In agreement with Ref. 34 the result is nearly zero for this special value. This value of Λ is also the point at which the $F(Z)$ plots (Fig. 4) start diverging with further decreases in Λ. At this special matching point little leakage of magnetism into the superconductor occurs. The importance of this crossover point becomes more evident in the remaining curves, where the mismatch parameter is decreased to $\Lambda=0.4$ and then to 0.1. The sign of the δN variations with energy is reversed. This pattern and the relatively large maximum and minimum values of δN reflect that the high peaks reached by the DOS at these values of Λ (see Fig. 5, right column) occur at slightly different values for the up and down spin bands. Again, the magnetic moment at those distances is very small: if one integrates the normalized δN over the variable ϵ/Δ_0, the result is of order 10^{-2} at $Z=\Xi_0$, changing sign at $\Lambda=2/3$. Only very near the interface, at values of Z of order unity, do we find that this integral is larger and, of course, always positive. As a rule, spin-splitting effects in the self-consistent DOS extend through several times ξ_0 (being larger near $\epsilon/\Delta_0=1$ for the reasons already discussed), except of course at the reversal point. The parameter characterizing the degree of wave vector mismatch is therefore important in the study of proximity effects on both sides of the F/S interface.

3. Interface scattering

Up to this point we have considered only transparent interfaces. A thin oxide layer at the interface adjoining a superconductor and a normal metal or ferromagnet can be modeled by a repulsive δ function potential as defined earlier in Sec. II. The spin-independent scattering strength is parametrized in dimensionless units by the quantity H_B, defined in Table I. Here we summarize the salient results of the inclusion of this parameter. Reference 39 can be consulted for further details. We concentrate on the case of fairly low temperatures and mismatch parameter close to unity for this discussion.

At $I=0$, $F(Z)$ still decays slowly into the normal side, but with an overall large decrease in amplitude. The pair amplitude is adequately fit by the functional form of Eq. (12) but with the parameters c_1 and c_2 being both functions of H_B. There are Friedel-type[44] oscillations in $F(Z)$ near the interface: as the insulating barrier becomes stronger, the two parts of the system become more isolated from each other. Within the superconductor, the pair correlations within a range of order ξ_0 from the surface increase with increasing barrier strength. The oscillations near the interface have the same period as in the normal metal, and their amplitude increases with H_B. As in the previous subsection, $F(Z)$ is continuous at the interface.

At intermediate or large values of I, it is found that the amplitude of the damped oscillations decreases as the scattering potential is increased. The period is independent of H_B, in agreement with Eq. (14). The additional decay of the amplitude of the oscillations can be incorporated into Eq. (16) through a multiplicative factor that decreases linearly with H_B. The location of the first node of $F(Z)$ in the magnet is nearly unaffected, demonstrating that both the characteristic length scales $k_{FS}\xi_1$ and $k_{FS}\xi_2$ are independent of interface transparency. On the superconductor side, the length scale over which $F(Z)$ regains its bulk value from the interface decreases as the scattering potential increases. As the barrier becomes very strong (H_B of order unity) the proximity effects become of course minimal.

The local DOS is also modified by the finite barrier strength. At $I=0$, the general trend on increasing the scattering potential is a reduction in the magnitude of the peaks for subgap energies. The characteristic energy spacing E_c shows relatively little change, but the shape of the peaks[39] is altered. For the superconductor, the de Gennes–St. James bound states become smeared out as H_B increases, until at about $H_B=0.6$ the influence of the normal metal becomes almost nonexistent. Thus we find that although both the insulating barrier and the Fermi energy mismatch tend to destroy superconducting order in the nonsuperconductor, their DOS signature is quantitatively different.

At finite exchange fields, there is, for small H_B, a wide structure in the subgap DOS. Upon increasing the barrier strength there is a dramatic reduction in this structure. When the barrier strength is rather large ($H_B \geqslant 0.6$), the DOS on

the magnetic side shows very minimal signs of the proximity effect even very near the interface. On the superconductor side, a similar trend can be noted. One coherence length away from the interface, the subgap states at zero barrier gradually disappear with increasing H_B, while simultaneously sharp BCS peaks develop. For $H_B \geqslant 0.5$, the results follow closely the $I=0$ case since the influence of the nonsuperconductor material has vanished. These results illustrate the importance of fabricating samples with good, clean interfaces.

B. Structures

All of the above results pertained to "bulk" structures, in that both slabs were taken to have dimensions significantly larger than the zero-temperature BCS coherence length. We now address what happens when either the ferromagnet or the normal metal is thin enough so that size effects are appreciable. A bilayer system of this type is an appropriate model for the case when the mean free path in the finite layer is larger than the layer's width. We will present a broad range of results, varying D_F from a few atomic spacings up to of order Ξ_0, while keeping $D_S \gg \Xi_0$, and vice versa. We will consider the case where both D_F and D_S are small in Sec. III C. For the sake of brevity, we will take the interface to be transparent ($H_B=0$), the mismatch parameter to be $\Lambda=1$, and fix the temperature to $t=0.02$.

We begin with a normal metal ($I=0$) of finite width backed by a "bulk" superconductor, taken here to be $D_S = 16\Xi_0$. The top panel in Fig. 7 shows the pair amplitude in the superconductor for various normal metal widths. We show $F(Z)$ only for the superconductor side since the pair amplitude in the finite normal side is cut off at different distances. The top curve corresponds to a single superconductor slab (zero width for the normal metal), while subsequent curves are for increasing normal metal widths ranging up to $D_F=200$. The oscillations near the interface at zero or very small D_F are again the well-known geometrical Friedel oscillations. The largest changes in the pair amplitude near the interface occur for $0<D_F<20$. When $D_F \geqslant 50$, the characteristic length scale for superconducting depletion is given approximately by the coherence length ξ_0. The inset displays Δ_{MIN} [as usual, the value of $\Delta(Z=0)$] as a function of D_F. It is seen that Δ_{MIN} drops rapidly until about $D_F=50 = \Xi_0$ and thereafter it decays more slowly.

The same geometry as in the top panel of Fig. 7 but with the finite nonsuperconducting layer being ferromagnetic ($I=1/2$) is considered in the bottom panel of this figure, which again depicts the pair amplitude in the superconductor. As the ferromagnet thickness D_F begins to increase from zero the pair amplitude drops very rapidly, as in the $I=0$ limit. A notable distinction exists here, however. When D_F is larger than about $D_F=10$, the characteristic length scale over which $F(Z)$ rises to its bulk value becomes approximately independent of D_F. This behavior is also seen in more detail in the inset of the same figure where we plot Δ_{MIN} as a function of D_F. The decay of Δ_{MIN} occurs nearly entirely in the region $D_F \leqslant 10$, while for $I=0$ it takes place over a much more extended range. This of course reflects that the superconducting penetration (at low T) into the normal metal is very large, while for a magnet with $I=1/2$ it is characterized by a length of order ξ_2. Once D_F reaches that limit, further increases are ineffective.

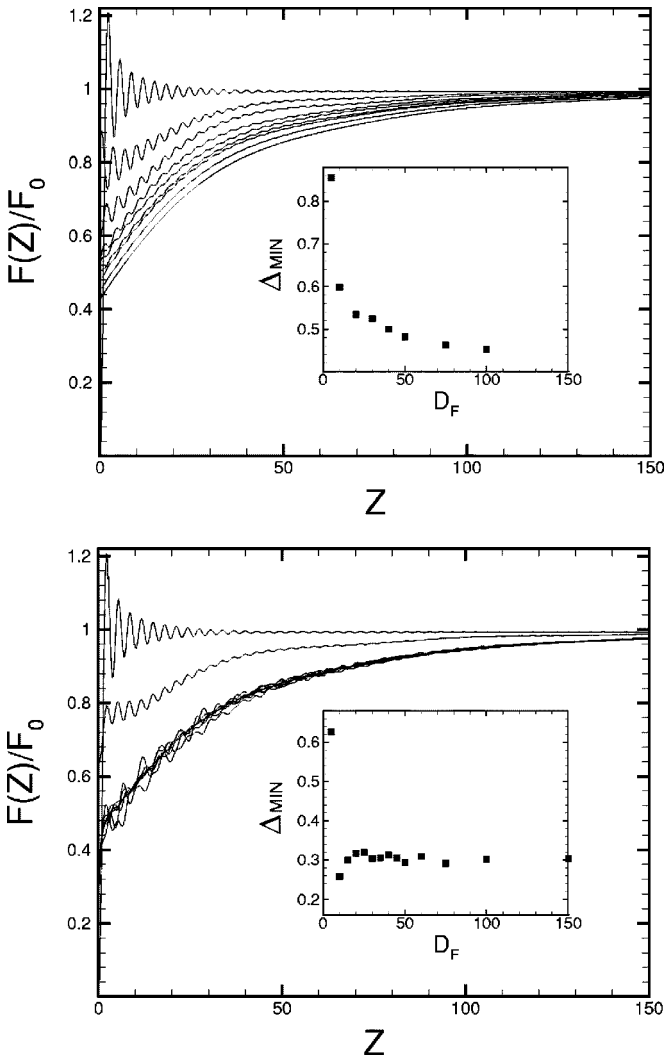

FIG. 7. Pair amplitude in a superconductor in proximity to a nonsuperconducting layer of finite thickness D_F (see text). The top panel shows results for $I=0$. The curves from top to bottom correspond to $D_F=0,5,10,20,30,40,50,100,200$, respectively. The bottom panel has results for $I=1/2$. The top two curves are for $D_F=0,5$. The other curves, all of which essentially coincide, are for the remaining values of D_F as shown in the top panel. The insets show Δ_{MIN} vs D_F in each case.

We have also calculated the DOS for the geometries used in Fig. 7. Since the nonsuperconductor layer is in some cases quite thin ($D_F<\Xi_0$), the local DOS in the normal region exhibits strong oscillations as a function of Z. For this reason, we present results for the spatial average of $N(Z,\epsilon)$ over a distance in the Z direction equal to the layer thickness D_F if $D_F<\Xi_0$ or over one dimensionless coherence length Ξ_0 if $D_F>\Xi_0$. In the latter case this average is centered at $Z = -D_F+\Xi_0/2$. We present in the two top panels of the left column of Fig. 8, the averaged DOS within the normal ($I=0$) metal for two different thicknesses, at $t=0.02$. The top

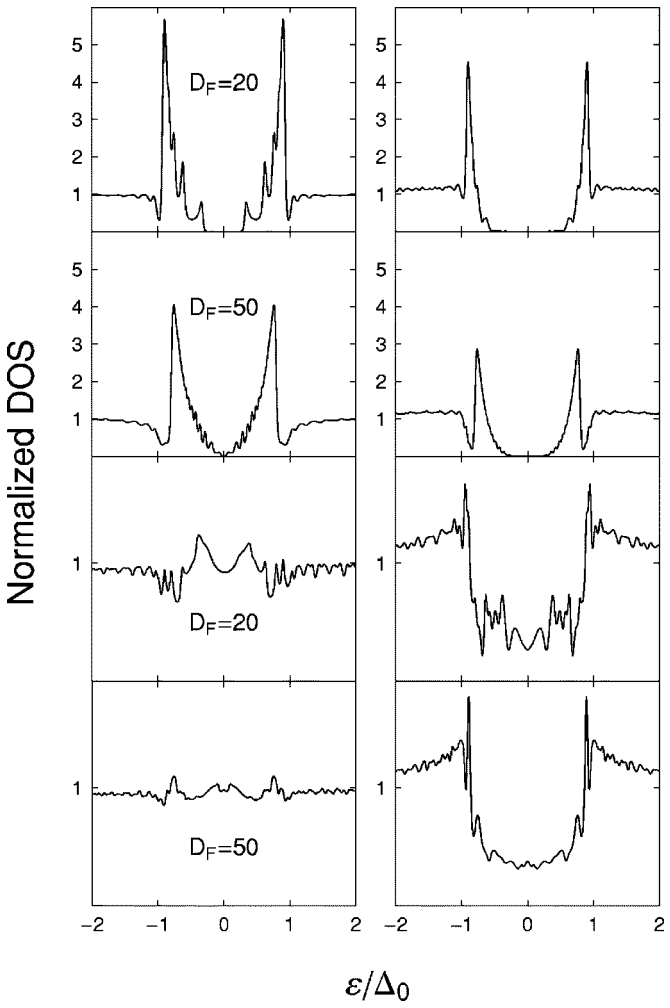

FIG. 8. Local DOS for the same geometry analyzed in Fig. 7. The top four panels are for $I=0$ and the bottom four are for $I=1/2$. The panels in the left column show the normalized local DOS in the nonsuperconductor, spatially averaged over one Ξ_0 as described in the text, for the indicated values of D_F. The right column contains the respective local DOS at $Z=50$ in the superconductor, for the same values of D_F as in the left column.

left panel corresponds to a thin film with $D_F=20$ (recall that the superconductor is in the bulk limit). A clear ''minigap'' structure is present. As D_F is increased to $D_F=50$, the gap decreases and multiple bound-state ripples rise to two larger peaks. We find that there exists a maximum thickness for the normal metal, $D_F \approx \Xi_0$, such that, if exceeded, the gap in the normal side DOS disappears. The observed filling in of the states originates from quasiparticles with relatively large momenta parallel to the interface ($k_\perp \approx k_{FS}$). In the two top panels of the right column of Fig. 8, the corresponding local DOS in the superconductor is shown. Here we need not spatially average the local DOS, since we are in the bulk regime and the DOS varies smoothly. We present the local DOS at $Z=\Xi_0$, while all other parameters take the values used in the left column. The top curve ($D_F=20$) shows a widening of the gap, while the main peaks still remain below $\epsilon/\Delta_0=1$. As D_F increases to $D_F=50$, the bound-state peaks are pushed further towards the Fermi level. Although not shown, the DOS structure evolves to that of a BCS form deep within the superconductor.

The case where the nonsuperconductor layer in the system is a ferromagnet is presented in the four bottom panels of Fig. 8, still at $t=0.02$ and $I=1/2$. In the magnetic side, we spatially average the DOS over its width D_F as described above. The result is shown in the two bottom panels of the left column of Fig. 8. The curve for $D_F=20$ exhibits two slightly asymmetric peaks at $\epsilon/\Delta_0 \approx 0.2$. The structure seen there is washed out at the larger $D_F=50$, as seen in the bottom left panel. There is no gap in the ferromagnet DOS shown but we found[39] a minigap when D_F is small ($D_F \approx k_{FS}\xi_2$). The corresponding DOS at the point $Z=\Xi_0$ inside the superconductor is illustrated in the right column of Fig. 8. In the third panel from the top ($D_F=20$), it is seen that the higher most peaks are shifted slightly towards lower energies ($\epsilon/\Delta_0 \approx 0.9$) compared with the bulk BCS result. At even lower energies there are subgap states. These states disappear at $D_F=50$, as one can see in the bottom curve. We find that the presence of the magnet next to the superconductor results in more prominent features in the DOS, at smaller D_F values.

We now reverse the role of the two materials in the bilayer; that is, we consider a very thick ''bulk'' ferromagnet (we take $D_F=16\Xi_0$ as was done above for D_S), in contact with a finite superconductor layer. Temperature and other parameters are as in the previous case. In order to study fully the geometrical effects associated with varying the superconductor thickness, we shall consider a wide range of widths D_S, taking Ξ_0 close to the lower bound, since the superconductor ceases to maintain pairing correlations when $D_S \lesssim \Xi_0$.

The top panel of Fig. 9 shows the modification of the pair correlations in a bulk normal metal ($I=0$) that occur as the width of the superconductor varies. The top curve ($D_S=4\,\Xi_0$) differs relatively little from the situation discussed above, where both the normal metal and superconductor were in the bulk. A decreasing trend is followed as D_S decreases. The slow decay of $F(Z)$ away from the interface is adequately fit by Eq. (16) for $D_S \geqslant 1.5\,\Xi_0$, the only modification being an overall D_S-dependent factor that reduces the amplitude. The bottom two curves, corresponding to $D_S=0.9\,\Xi_0, \Xi_0$, have an even slower decay. The inset depicts the corresponding change in the pair potential at the interface, Δ_{MIN}, as a function of D_S. This inset emphasizes the fast rise in the pairing correlations at the interface when D_S is on the scale of Ξ_0, and it includes additional values of D_S not presented in the main plot. In the bottom panel of Fig. 9 we show the damped oscillations of $F(Z)$ within the ferromagnet ($I=1/2$) for the same values of D_S as in the top panel. The main effect of changing D_S is to reduce the amplitude of the oscillations while their period remains, as expected, the same. Their amplitude, however, drops very markedly when D_S approaches Ξ_0. This is illustrated in the inset, where we display Δ_{MIN} versus D_S. The essential behavior is similar to that in the $I=0$ case in the other panel,

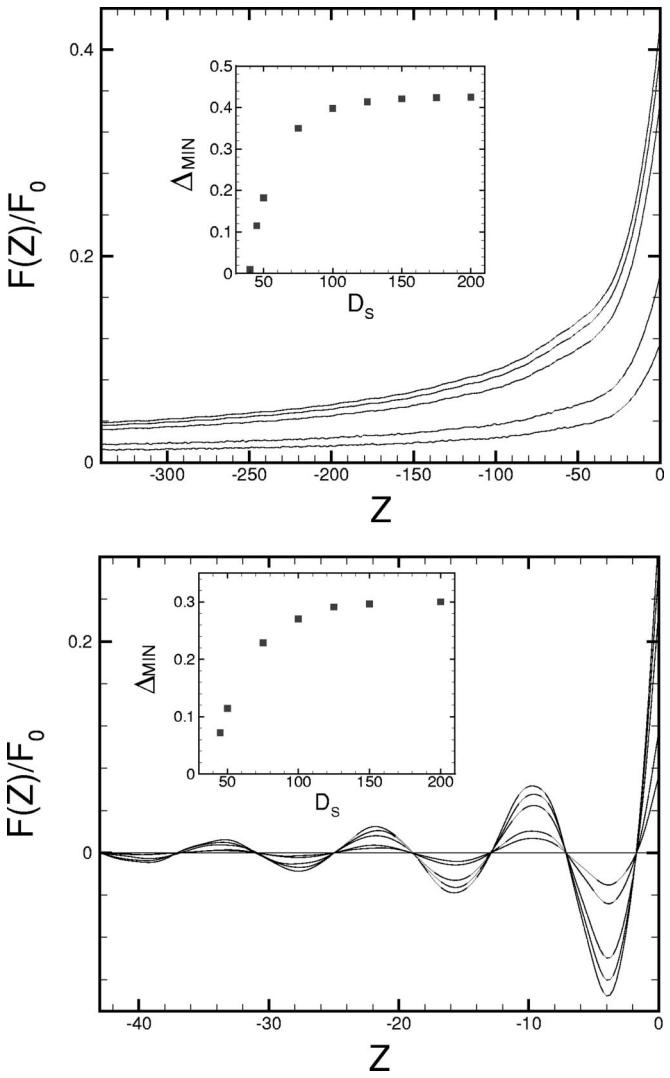

FIG. 9. Pair amplitude a structure consisting of a superconductor of finite thickness D_S adjoining a thick nonsuperconductor. The main plot in the upper panel shows the decay of the pair amplitude in the normal metal ($I=0$) for values of $D_S=200,100,75,50,45$ (from top to bottom). The lower panel shows the pair amplitude at $I=1/2$ and the same geometry. The values of D_S are the same as in the top panel, and the amplitude of the oscillations decays with decreasing D_S. The insets illustrate the behavior of Δ_{MIN} vs D_S in each case.

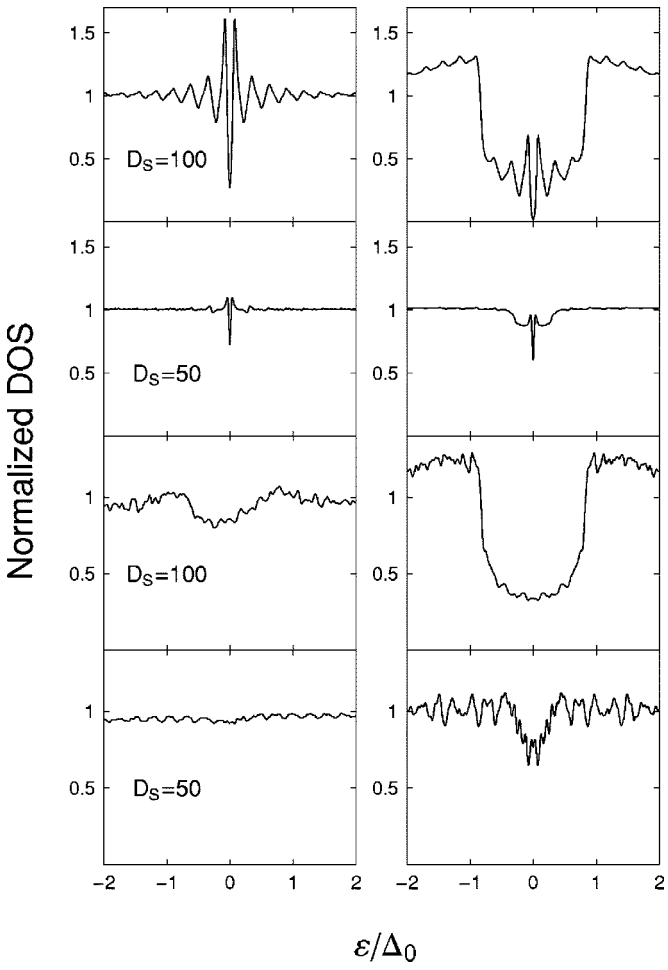

FIG. 10. Local DOS results for a structure consisting of a superconductor of finite thickness D_S adjoining a thick nonsuperconductor. The top four panels are for $I=0$ and the bottom four for $I=1/2$. The left column corresponds to the nonsuperconductor, at $Z=-100$ for the top two rows and $Z=-3$ for the bottom two. The value of the thickness D_S is indicated in the labels. The right column depicts the local DOS for the same structure, averaged over one Ξ_0 (see text) from the end of the superconductor, for the same D_S values as in the left column.

whereby Δ_{MIN} changes the most for $D_S<1.5\ \Xi_0$. The overall magnitude is reduced, however, by the finite value of the exchange energy.

The local DOS is also sensitive to the spatial extent of the superconductor. This is shown in Fig. 10. The left column in this figure contains results for the normalized local DOS in the nonsuperconducting side, while in the right column we examine the DOS in the superconducting side, using the same parameters as for the left side panels. In the superconducting side we perform a spatial average over one coherence length centered around $Z=D_S-\Xi_0/2$ (in analogy with the thin magnet case). The top four panels are for $I=0$. In this case the left column contains results at $Z=-100$. Spatial averaging is then unnecessary. For $D_S=100=2\Xi_0$ (top left panel), it is evident that this width is sufficient for coherent Andreev reflection to become well established and, hence, for the formation of a structure recognizable as similar to that described for the bulk case. However, at $D_S=\Xi_0$ (second panel from left top), only a slight hint of structure remains. These results reflect that the de Gennes–St. James peaks arise mainly from Andreev reflection at the normal-metal–superconductor interface, so that when D_S decreases, so does the minimum gap (see Fig. 9, inset in the top panel). On the right side, we see the DOS in the superconductor, averaged as explained above. As D_S is decreased from $D_S=100$ (top right) to $D_S=50$ (second from top right), any remnant of subgap states becomes filled in due to the greater influence of the normal metal on the superconductor for smaller D_S.

The bottom four panels of Fig. 10 show results at $I=1/2$, with all other material parameters being identical to

those in the top four panels. We present in the two bottom panels of the left column, the local DOS at the position $Z=-3$ for two values of D_S. For $D_S=2\Xi_0$, the DOS profile has two rounded peaks near the gap edge, while the minimum is near $\epsilon/\Delta_0\approx 0$. This is fairly similar to what was seen at the same distance in Fig. 2. To understand the behavior of the DOS for smaller D_S, we recall the spatial dependence of the pair correlations in Fig. 9. There it was found that the oscillations in $F(Z)$ did not undergo a change in period as the superconductor width decreased. Rather, there was a smooth reduction in amplitude as D_S decreased. This suggests that changes in the DOS with decreasing D_S would behave similarly. The bottom panel in the left column of Fig. 10 agrees with this reasoning: the effect of reducing D_S is to lower peaks and raise minima, so that the leakage of superconducting order is effectively eliminated when $D_S=\Xi_0$. The two bottom panels in the right column of Fig. 10 show the corresponding DOS in the superconductor, averaged over a distance of one Ξ_0 in the usual way. The third panel from the top ($D_S=2\Xi_0$, so that the average is taken centered at $Z=75$) shows a clear reduction in subgap states and little variation in the DOS for $\epsilon/\Delta_0>1$. When $D_S=\Xi_0$, (bottom panel) there is hardly any evidence of the previous superconducting structure, indicating that superconductivity is nearly destroyed as the thickness is down to one correlation length.

C. Comparison with experiment

We have seen above that the calculated self-consistent results for the physical quantities depend in a systematic way on a number of parameters, some of which are related to the materials employed, while others are experimentally adjustable. While testing these systematic dependences is the task of future experimental work, we will, in this subsection, compare already existing data with our theory. We will use data from direct local DOS measurements[3,37] rather than results for indirectly derived quantities. Although we heavily emphasize in this work the case where the nonsuperconductor is a ferromagnet, we will examine also the proximity effect when the ferromagnet is a normal metal. We will thus compare our calculations with the experimental data of Ref. 37, where DOS measurements were made from the normal metal side, and with data from Ref. 3, where local DOS measurements in the superconductor side of a magnet-superconductor structure were taken. In this way, we test our theory against spectroscopy data obtained by probing either side of the interface, in the two cases where the superconductor is in proximity to either a normal metal or a strong magnet. In making our comparisons, it is important to make pertinent choices for the applicable input parameters, as will be discussed below.

Consider first the STM data of Ref. 37, where the superconductor (Nb) is in contact with a nonmagnetic metal (Au). The experimental configuration consisted of a thin layer of Au of thickness 200 Å, which capped off a superconducting Nb dot. The Nb had a smooth relief resulting in a thickness (0–400 Å) that decreased away from its center. We model this structure, as done in the experimental analysis,[37] as a bilayer system comprised of a normal metal of constant width on a superconductor of varying thickness in the z direction, in a manner similar to Sec. III B. We take $k_{FM}=1$ Å^{-1}, and we assume the normal metal to have a width of 200 Å. The transition temperature is $T_c=9$ K. We assume the temperature to be $T=270$ mK, a value which is slightly higher than the experimental value $T=60$ mK. This is intended, in the usual way, to account for additional smearing effects associated with the finite energy resolution of the apparatus. The interfacial barrier strength parameter (H_B) is taken to be zero, which is appropriate for the clean, highly transparent interface used, and the Fermi wave vectors in the two materials are assumed to be equal. Other parameter values used in our calculations are the bulk Nb gap value $\Delta_0=2$ meV, which is close to the experimental value,[37] and the Debye cutoff parameter $\omega=0.03$, the value of this parameter having little effect on the results. The modeling of the superconductor width is less trivial since the Nb dot in fact varies in size not only in the z direction, but also in the transverse direction. With this in mind, we assume a superconductor thickness varying from 50 to 150 Å. Because of possible nonuniformities in the composition of the Nb dot, this quantity should be viewed as an effective thickness that accounts for any geometrical discrepancies between our model and the experimental configuration, and which may be interpreted to some extent as a fitting parameter. The final physical parameter needed is the coherence length ξ_0. This parameter must be identified here as an effective correlation length to absorb the inherent effects of disorder in the system. Measurements were taken at several points: some [which were labeled as points $a-d$ in Fig. 1(a) of Ref. 37] were on the flatter part near the center of the dot. The others, labeled $e-j$ in that figure, were in the sloping part near the edge. Disorder effects are likely to be more prevalent in the region in the latter points, where oxidation of the sample surface has a more pronounced effect on the superconducting order. Therefore we have set at $\xi_0=100$ Å in the region corresponding to the points $e-j$, while for in the region between the points $a-d$ we take $\xi_0=200$ Å. These two sets of points were recognized as behaving differently in the original experimental analysis.[37]

The geometry studied is not quite that in our earlier results of Sec. III B, where we varied the width of the superconductor in contact with an *infinite* normal metal. Here, both the normal metal and superconductor are effectively thin, and additionally, the assumed value of the coherence length is larger. Therefore, separate computations were required. We present in Fig. 11 the comparison of our results (solid line) to the experimental data.[37] The DOS is scaled to its normal metal limit, with the curves shifted by a constant for illustrative purposes. The energy is in the same voltage units as in the experiment. Inspecting the spectra corresponding to the points $a-d$ (labeled in our figure as they were in the experimental work), Fig. 11 demonstrates the excellent agreement between our results and the data. In the top panel, a BCS-like gap is most evident for the position the location labeled a, and as the effective superconductor width is decreased from 150 Å in a to 120 Å in d, the gap becomes smaller, while the BCS peaks decrease in magnitude. The locations of the peaks in the fits and in the experimental data

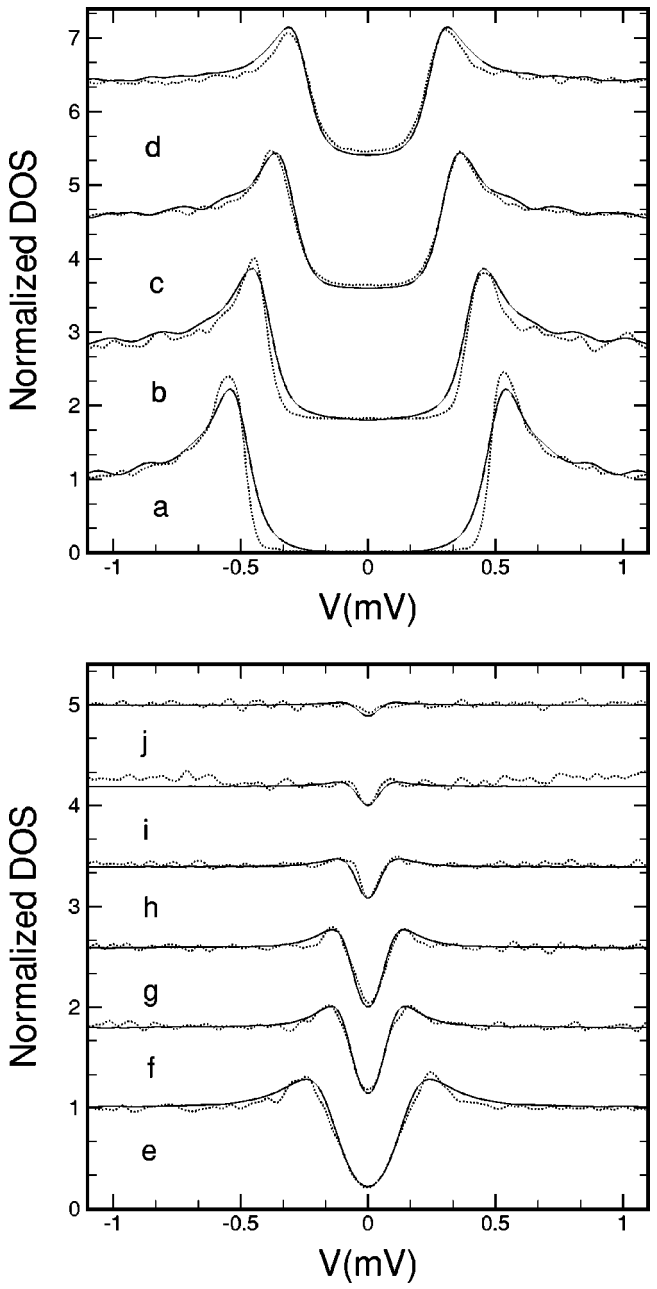

FIG. 11. Comparison of experimental STM data from Ref. 37 with theory. The solid curves are our theoretical results and the dotted curves the experimental data. The vertical axis scales have been shifted for clarity. The labels $a-j$ correspond to different probe positions on the sample: they are the same labels as used in the experimental work. See text for details.

are seen to essentially agree. A similar trend is seen for the remaining probe locations in the bottom panel of Fig. 11, where the effective coherence length and D_S are smaller. The peaks move inwards while the previously empty gap starts to fill in, with an approximately linear rise near the Fermi level. This DOS profile is observably different from that in the panel above, where the subgap DOS had a U shape compared to the V shape here. It is remarkable that the level of agreement between theory and experiment is so high, in that the location of the peaks as well as the origin of the minima in the DOS match well over the entire spatial range. Thus we find that modeling this particular experimental structure as a bilayer is successful over the entire spatial range. In Ref. 37 it was found that a fit to all the data using the Usadel equations was not possible and that very different physical assumptions had to be used for the U- and V-shaped portions. This is unnecessary within the exact theory.

When the normal metal is a ferromagnet, experimental studies on the proximity effect are more sparse. The continuing advancement in nanofabrication techniques, however, has made probing the electronic structure of F/S nanostructures experimentally accessible and some recent good-quality data are available. We compare our theory with the tunnel spectroscopy data of Ref. 3 obtained through probing the local DOS in an Al superconductor adjacent to a Ni ferromagnet. Modifications to the DOS in the superconductor are another important aspect of the proximity effect which provides useful information regarding the influence of the ferromagnet on superconducting correlations. As predicted in Sec. III A 1 the local DOS near the interface in the superconductor should be substantially modified from the bulk BCS result. It is then of great interest to see how our results compare with the appropriate experiment.

To test our theory against the Al-Ni experimental data, we must choose a set of parameters appropriate for the given bilayer. Nickel itself is not a simple Stoner magnet with parabolic bands. A nearly free electron monovalent metal having the same saturation magnetization[45] as Ni is easily seen to be to have a value of I of about 0.5 and this is the value we will use. We assume a transparent interface ($H_B=0$) in accordance with the clean interface in the experiment.[3] We also take $T_c=1.2$ K, $k_{FM}=0.5$ Å^{-1}, and in order to limit as much as possible the number of input parameters, we keep the Fermi wave vectors the same, $\Lambda=1$. For thick superconducting layers the relevant length which governs the depletion of superconducting correlations near the interface[34] scales with ξ_0 whenever $\Xi_0 \gg 1$. In the experimental work, distances were already given in units of the correlation length, and this makes it particularly convenient to compare with theory. Experimental data are given at two distances: one far from the interface and the other near to it. The precise distance from the tunneling probe to the interface in the second case was somewhat uncertain, however, mainly because of the finite width of the probe. We take this position to be $2\,\xi_0$, which is similar to the value estimated in the experimental analysis.[3]

Figure 12 shows a fit of our results (solid lines) to the experimental data of Ref. 3. The vertical axis is the DOS scaled to the normal state value, while the energies are in dimensionless units of ϵ/Δ_0. We account for the influence which single-charging effects have on the DOS by convolving the DOS calculated from Eq. (9) with the acceptance function $P(E)$ (as described in Ref. 3) that gives the probability for the junction to absorb an energy E.[46] The curve with the more prominent peak corresponds to the DOS in the bulk, away from the influence of the magnet, while the other curve is the DOS two coherence lengths from the interface. The open and solid symbols are the experimental results, the former ones being for the bulk DOS. The procedure em-

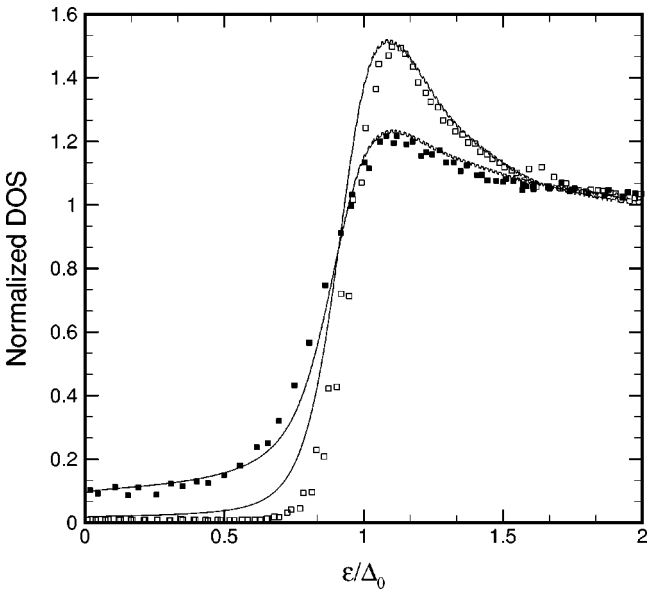

FIG. 12. Comparison of experimental DOS data for Ni-Al structure (Ref. 3) with theory. The symbols represent data taken far from the interface (open symbols) and near it (solid symbols). The curves are the theoretical fits obtained as explained in the text.

ployed to obtain these fits was the following: first we determined the effective temperature (to account for instrument resolution) by fitting our results to the experimental DOS near the interface (solid symbols, solid curve). This resulted in a slightly raised effective temperature $T=980$ mK (in contrast with the experimental value of $T=100$ mK). Then, without any further changes, we calculated the DOS at a distance of 4 ξ_0 from the interface (dashed curve). This position should represent well the bulk characteristics in the DOS, since as we have seen previously, at that point, the influence of the ferromanget on the superconducting DOS is minimal. No additional parameters were used to obtain this second fit. The results are clearly excellent: they have the correct peak positions and relative magnitudes. We therefore find, again, good overall agreement with experiment in this more difficult case.

IV. CONCLUSIONS

We have in this work presented extensive results for the pair amplitude and local DOS in heterostructures involving superconductors and magnetic materials. These results were obtained from numerical, self-consistent solution of the Bogoliubov–de Gennes equations, without approximations. We also discussed the length scales characterizing the influence of the superconductor on the ferromagnet and vice versa.

For heterostructures with geometric dimensions larger than the relevant intrinsic lengths, we have shown in detail how variation of parameters such as temperature T, Fermi wave vector mismatch Λ, and interfacial and scattering strength H_B (see Table I) affected the pair amplitude and local DOS for a wide range of exchange energies I. For $I=0$ and low T, we find that the pair amplitude in the normal metal decays approximately as the inverse of the distance from the interface, with the overall prefactor depending on Λ and H_B. At higher temperatures and for $\Lambda=1$, $H_B=0$, the decay markedly increases and is set by a smaller length scale $\xi_N(T)$. The exact spatial decay of $F(\mathbf{r})$ was found to be more complicated than a single exponential. On the superconductor side, we tested our results for temperatures near T_c and found agreement with standard Ginzburg-Landau theory. We also extracted the characteristic length of depletion $\xi_S(T)$ for intermediate and lower temperatures, something not previously done in a systematic way. The length scale (at low temperatures) characterizing the decline of $F(\mathbf{r})$ near the interface was found to decrease with smaller Λ or larger H_B. The local DOS correlates with these results and displays a functional dependence on T, Λ, and H_B as well. We also systematically investigated the geometrical effects associated with the finite size of either the normal metal or superconductor and discovered that a small gap develops in the normal metal DOS when its width is small. This ''minigap'' decreases to zero when the metal width is close to the coherence length, i.e., $D_F \approx \Xi_0$.

At finite values of I, there are two characteristic proximity length scales ξ_2 and ξ_1 in the ferromagnet, governing, respectively, the spatial period of the damped oscillations in $F(\mathbf{r})$ and the sharp decay at the interface. Both lengths vary approximately inversely with I, independent of temperature. The amplitude of the damped oscillations, however, decreases with increasing temperature. Mismatch of the Fermi energies increases the decay of the oscillations. A finite barrier strength has no effect on the period either, but does reduce the amplitude by a factor that scales linearly with H_B.

The damped oscillatory behavior in the ferromagnet induces a corresponding spatial modulation in the local DOS. For a transparent interface, the DOS in the superconductor side (for $I>1/4$) exhibited a reduction in the usual BCS peaks, with a finite number of states within the gap, the number depending on the exchange field and location within the superconductor. For small exchange fields of order of $I \simeq \Delta_0/E_{FS}$, a significant subgap structure emerged and, at exactly $I=\Delta_0/E_{FS}$, a resonance phenomenon occurred in which the BCS peaks became significantly enhanced. We found there exists a long-range spin splitting in the superconductor, extending over several coherence lengths. A nontrivial behavior of δN was found as a function of I and the mismatch parameter Λ: when the point $E_{F\uparrow}=E_{FS}$ is crossed, the spin splitting becomes very short ranged, as found in Ref. 34.

Finally, we have compared our results with two sets of experimental data for the local DOS, corresponding to two different values of I and to measurements taken either from the superconductor or the nonsuperconductor side of the heterostructure. In both cases we found, using reasonable values for the material and geometric parameters, very good agreement between theory and experiment.

The only approximation made here is that of assuming the clean limit. It is of interest to briefly consider how the inclusion of scattering would affect the results. We have mentioned in Sec. III C that the coherence length would have to

be replaced by its effective value. One can risk some further speculation by comparing with existing work[25,47] within the Eilenberger approximation. Unfortunately, in these semiclassical papers Δ is not determined self-consistently, so our comments must remain very tentative. The main periodicity of the oscillatory behavior appears to be independent of the impurity mean free path l and still given by $(k_{F\uparrow}-k_{F\downarrow})^{-1}$. The relevant dimensionless parameter for impurities is, in our notation, Ik_Fl, as one would expect. The main effect of a finite l appears to be that the amplitude decays of oscillatory quantities contain a damping factor $\approx e^{-2z/l}$. However, we have found (see, e.g., Fig. 1) that there is a marked amplitude decay even in the clean limit, which should dominate the effect of impurities except for rather short l. Hence it appears that our results should remain valid for reasonably clean samples.

In summary, the number of relevant parameters involved is so large and the variety of behaviors so rich that a study such as this one must concentrate on the highlights and leave most of parameter space unexplored. It is clear, however, that the machinery developed here can be readily applied to most actual experimental situations. We hope that this paper will stimulate future experimental work and facilitate the analysis of the resulting data.

ACKNOWLEDGMENTS

We thank H. Courtois and M. A. Sillanpää for providing us with their data.

*Electronic address: khalter@physics.umn.edu
†Electronic address: otvalls@tc.umn.edu

[1] P.A. Kraus, A. Bhattacharya, and A.M. Goldman, Phys. Rev. B **64**, 220505 (2001).
[2] A.N. Grigorenko *et al.*, Phys. Rev. B **63**, 052504 (2001).
[3] M.A. Sillanpää, T.T. Heikkila, R.K. Lindell, and P.J. Hakonen, Europhys. Lett. **56**, 590 (2001).
[4] G. Deutscher and P.G. de Gennes, in *Superconductivity*, edited by R.D. Parks (Marcel Dekker, New York, 1969), p. 1005.
[5] D.S. Falk, Phys. Rev. **132**, 1576 (1963).
[6] P.G. de Gennes, *Superconductivity of Metals and Alloys* (Addison-Wesley, Reading, MA, 1989).
[7] B.P. Stojković and O.T. Valls, Phys. Rev. B **50**, 3374 (1994).
[8] J. Hara, M. Ashida, and K. Nagai, Phys. Rev. B **47**, 11 263 (1993).
[9] E.A. Demler, G.B. Arnold, and M.R. Beasley, Phys. Rev. B **55**, 15 174 (1997).
[10] Y. Blum, A. Tsukernik, M. Karpovski, and A. Palevski, Phys. Rev. Lett. **89**, 187004 (2002).
[11] V. Prokic, A.I. Buzdin, and L. Dobrosavljevic-Grujic, Phys. Rev. B **59**, 587 (1999).
[12] F.S. Bergeret, A.F. Volkov, and K.B. Efetov, Phys. Rev. B **64**, 134506 (2001).
[13] L.N. Bulaevskii and V.V. Kuzii, JETP Lett. **25**, 290 (1977).
[14] A.I. Buzdin, L.N. Bulaevskii, and S.V. Panyukov, JETP Lett. **35**, 178 (1982).
[15] A.I. Buzdin, B. Bujicic, and M.Yu Kupriyanov, Sov. Phys. JETP **74**, 124 (1992).
[16] P. Fulde and A. Ferrell, Phys. Rev. **135**, A550 (1964).
[17] A. Larkin and Y. Ovchinnikov, Sov. Phys. JETP **20**, 762 (1965).
[18] Z. Radovic *et al.*, Phys. Rev. B **44**, 759 (1991).
[19] L.R. Tagirov, Physica C **307**, 145 (1998).
[20] Y.V. Fominov, N.M. Chtchelkatchev, and A.A. Golubov, Phys. Rev. B **66**, 014507 (2002).
[21] T. Kontos *et al.*, Phys. Rev. Lett. **89**, 137007 (2002).
[22] V.V. Ryazanov *et al.*, Phys. Rev. Lett. **86**, 2427 (2001).
[23] M. Krawiec, B.L. Gyorffy, and J.F. Annett, cond-mat/0203184 (unpublished).
[24] Ya.V. Fominov and M.V. Feigelman, Phys. Rev. B **63**, 094518 (2001).
[25] I. Baladie and A. Buzdin, Phys. Rev. B **64**, 224514 (2001).
[26] M. Zareyan, W. Belzig, and Yu.V. Nazarov, Phys. Rev. Lett. **86**, 308 (2001).
[27] K.D. Usadel, Phys. Rev. Lett. **25**, 507 (1970).
[28] G. Eilenberger, Z. Phys. **214**, 195 (1968).
[29] Y. Tanaka and M. Tsukada, Phys. Rev. B **42**, 2066 (1990).
[30] I. Žutić and O.T. Valls, Phys. Rev. B **61**, 1555 (2000).
[31] B.P. Vodopyanov *et al.*, Physica C **366**, 31 (2001).
[32] O. Bourgeois *et al.*, Phys. Rev. B **63**, 064517 (2001).
[33] J. Aarts *et al.*, Phys. Rev. B **56**, 2779 (1997).
[34] K. Halterman and O.T. Valls, Phys. Rev. B **65**, 014509 (2002).
[35] J-X. Zhu and C.S. Ting, Phys. Rev. B **61**, 1456 (2000).
[36] E. Vecino, A. Martin-Rodero, and A. Levy Yeyati, Phys. Rev. B **64**, 184502 (2001).
[37] N. Moussy, H. Courtois, and B. Pannetier, Europhys. Lett. **55**, 861 (2001).
[38] J.B. Ketterson and S.N. Song, *Superconductivity* (Cambridge University Press, Cambridge, England, 1999). See Chap. 41.
[39] K. Halterman, Ph.D. thesis, University of Minnesota, 2002.
[40] P.G. de Gennes and D. St.-James, Phys. Lett. **4**, 151 (1963).
[41] S. Pilgram, W. Belzig, and C. Bruder, Phys. Rev. B **62**, 12 462 (2000).
[42] R. Fazio and C. Lucheroni, Europhys. Lett. **45**, 707 (1999).
[43] G.E. Blonder, M. Tinkham, and T.M. Klapwijk, Phys. Rev. B **25**, 4515 (1982).
[44] B.P. Stojković and O.T. Valls, Phys. Rev. B **47**, 5922 (1993).
[45] See Chap. 15 in C. Kittel, *Introduction to Solid State Physics*, 7th ed. (Wiley, New York, 1996).
[46] G.-L. Ingold and Yu. Nazarov, in *Single Charge Tunneling*, edited by M.H. Devoret and H. Grabert (Plenum, New York, 1992).
[47] F.S. Bergeret, A.F. Volkov, and K.B. Efetov, Phys. Rev. B **65**, 134505 (2002). This work, which became available after the original version of our paper was submitted, uses the same basic (semiclassical, non-self-consistent) methods as Ref. 25, but covers a wider range of values of the parameter Ik_Fl.